View metadata, citation and similar papers at core.ac.uk

brought to you by CORE

provided by Northumbria Research Link

Northumbria Research Link

Citation: Valeyev, Najil, Kim, Jung-Su, Heslop-Harrison, Pat, Postlethwaite, Ian, Kotov, Nikolay and Bates, Declan (2009) Computational modelling suggests dynamic interactions between Ca2+, IP3 and G protein-coupled modules are key to robust Dictyostelium aggregation. Molecular BioSystems, 5 (6). pp. 612-628. ISSN 1742-206X

Published by: Royal Society of Chemistry

URL: http://dx.doi.org/10.1039/B822074C

This version was downloaded from Northumbria Research Link: http://nrl.northumbria.ac.uk/9682/

Northumbria University has developed Northumbria Research Link (NRL) to enable users to access the University's research output. Copyright © and moral rights for items on NRL are retained by the individual author(s) and/or other copyright owners. Single copies of full items can be reproduced, displayed or performed, and given to third parties in any format or medium for personal research or study, educational, or not-for-profit purposes without prior permission or charge, provided the authors, title and full bibliographic details are given, as well as a hyperlink and/or URL to the original metadata page. The content must not be changed in any way. Full items must not be sold commercially in any format or medium without formal permission of the copyright holder. The full policy is available online: http://nrl.northumbria.ac.uk/policies.html

This document may differ from the final, published version of the research and has been made available online in accordance with publisher policies. To read and/or cite from the published version of the research, please visit the publisher's website (a subscription may be required.)

www.northumbria.ac.uk/nrl

View Online / Journal Homepage / Table of Contents for this issue

Computational modelling suggests dynamic interactions between Ca^{2+}, IP_3 and G protein-coupled modules are key to robust *Dictyostelium* aggregation

Najl V. Valeyev,*[a] Jung-Su Kim,[b] J. S. (Pat) Heslop-Harrison,[ac] Ian Postlethwaite,[a] Nicolay V. Kotov[d] and Declan G. Bates[a]

Received 11th December 2008, Accepted 3rd March 2009
First published as an Advance Article on the web 16th April 2009
DOI: 10.1039/b822074c

Downloaded by University of Northumbria on 15 October 2012
Published on 16 April 2009 on http://pubs.rsc.org | doi:10.1039/B822074C

Under conditions of starvation, *Dictyostelium* cells begin a programme of development during which they aggregate to form a multicellular structure by chemotaxis, guided by propagating waves of cyclic AMP that are relayed robustly from cell to cell. In this paper, we develop and analyse a new model for the intracellular and extracellular cAMP dependent processes that regulate *Dictyostelium* migration. The model allows, for the first time, a quantitative analysis of the dynamic interactions between calcium, IP_3 and G protein-dependent modules that are shown to be key to the generation of robust cAMP oscillations in *Dictyostelium* cells. The model provides a mechanistic explanation for the transient increase in cytosolic free Ca^{2+} concentration seen in recent experiments with the application of the calmodulin inhibitor calmidazolium (R24571) to *Dictyostelium* cells, and also allows elucidation of the effects of varying both the conductivity of stretch-activated channels and the concentration of external phosphodiesterase on the oscillatory regime of an individual cell. A rigorous analysis of the robustness of the new model shows that interactions between the different modules significantly reduce the sensitivity of the resulting cAMP oscillations to variations in the kinetics of different *Dictyostelium* cells, an essential requirement for the generation of the spatially and temporally synchronised chemoattractant cAMP waves that guide *Dictyostelium* aggregation.

Introduction

The social ameba *Dictyostelium discoideum* is widely recognised as an important biological model for the study of cell motility[1,2] and human disease,[3,4] as many of the core molecular signalling pathways governing *Dictyostelium* chemotaxis and migration appear to be conserved in higher organisms, and impaired chemotaxis is associated with a range of diseases including asthma, arthritis, atherosclerosis and a number of cancers.[5–8] The diverse modes of *Dictyostelium* behaviour range from single cell states to the formation of functionally different multicellular structures such as moulds, slugs and fruiting bodies.[9]

Previous computational studies have provided significant insight into the molecular mechanisms underlying *Dictyostelium* chemotaxis.[10] One of the first models developed was based on a set of rules for cAMP metabolism, release and cAMP diffusion-based cell migration.[11,12] The rule-based modelling of *Dictyostelium* movement was further developed into computer models of *Dictyostelium* aggregation in refs. 13–15. Other early models, which were developed before the role of G proteins was discovered, focussed on oscillations in ATP and cAMP concentrations[16,17] or on interactions between Ca^{2+} and camp.[18] A third set of models employed simplified reaction-diffusion equations.[19–21] A detailed explanation of how cAMP oscillations can arise in *Dictyostelium* based on a network involving G protein-coupled receptors was developed more recently in ref. 22 and 23.

While the above computational studies have significantly advanced our understanding of various aspects of *Dictyostelium* behaviour, there are a range of questions that still require further elucidation. It has been shown experimentally that the levels of intracellular Ca^{2+} and cAMP in *Dictyostelium* are tightly interconnected[24–27] and a number of experiments involving the application of calmidazolium (R24571), a calmodulin (CaM) inhibitor, to *Dictyostelium* have demonstrated a dramatic impact on the light scattering oscillations[26,28] which are one of the major characteristics of aggregation.[26,29] Ca^{2+} has also been shown to be directly involved in cell migration *via* the stretch-activated Ca^{2+} channels (SAC)s.[1] Previously developed models for *Dictyostelium* signalling and aggregation do not allow these phenomena to be investigated, however, as they all omit one or more of the networks involved. To address this issue, we have employed a modular approach to develop a new model for cAMP oscillations in *Dictyostelium* that explicitly incorporates networks involving intracellular calcium (Ca^{2+}), inositol 1,4,5-triphosphate (IP_3)

[a] *Systems Biology Lab, Department of Engineering, University of Leicester, University Road, Leicester, UK LE1 7RH. E-mail: najl.valeyev@googlemail.com*
[b] *Department of Control and Instrumentation Engineering, Seoul National University of Technology, 172 Gongneung 2-dong, Nowon-gu, 139-743, Seoul, Korea*
[c] *Department of Biology, University of Leicester, University Road, Leicester, UK LE1 7RH*
[d] *Biophysics & Bionics Lab, Department of Physics, Kazan State University, 420008, Kazan, Russia*

 This journal is © The Royal Society of Chemistry 2009

View Online

Downloaded by University of Northumbria on 15 October 2012
Published on 16 April 2009 on http://pubs.rsc.org | doi:10.1039/B822074C

and the G protein coupled receptor cAR1. The proposed model provides a new understanding of how Ca^{2+} alterations are translated into cAMP oscillations and of the observed effects on light scattering oscillations of CaM inhibitors. We also use our model to study the effects of SACs conductivity and external phosphodiesterase (PDE) concentration on the oscillatory regime of an individual cell. Finally, we show that our model provides a new example of what has become a key theme in recent Systems Biology research—apparent structural redundancy in the proposed model (since cAMP oscillations can be generated *in silico* using just the G protein-coupled module on its own,[22,23]) appears to have been deliberately engineered by nature to ensure greater levels of robustness to uncertainty in the elements of the overall system. In particular, inclusion of interactions between the different modules in the proposed model is shown to result in significantly improved robustness to variations in the kinetics of the extracellular cAMP feedback loop, a critical requirement in the very early stages of aggregation when the levels of extracellular cAMP are likely to be very low.

Results

A new model for cAMP oscillations in *Dictyostelium* exhibits spontaneous oscillations matching experimentally verified results and is entrained by surrounding cells

A new model for cAMP oscillations in *Dictyostelium* has been developed that explicitly incorporates multiple networks of proteins governing the directed migration of *Dictyostelium* cells during the transition from single cell to multicellular organism.[30,31] In particular, the molecular circuit regulating *Dictyostelium* chemotaxis along cAMP gradients has been modelled as three interconnected modules involving intracellular calcium (Ca^{2+}), inositol 1,4,5-triphosphate (IP_3) and the G protein-coupled receptor cAR1,[24,26,32–35] as shown in Fig. 1. When external cAMP binds to cAR1, the G-protein cascade activates intracellular adenylate cyclase (ACA).[36] Transiently activated cAR1 can also lead to the activation of adenylate cyclases *via* the MAP kinase (ERK2). Intracellular cAMP is produced by ACA and degraded by intracellular phosphodiesterase (RegA). ERK2 is inhibited by cAMP-dependent protein kinase A (PKA).[22,37] Inactivated ERK2 loses its ability to phosphorylate RegA, in turn boosting the level of RegA activity. cAMP release creates an extracellular feedback loop for the cell, and also provides a source of additional cAMP signals for other cells in the vicinity. In addition to diffusion, the external cAMP feedback loop is also diminished by the external PDE.

Based on the experimental results reported in ref. 24–27, we have considered cAMP production and degradation to be dependent on the level of intracellular Ca^{2+}, which in turn is determined by a balance of fluxes into the cytoplasm from extracellular medium and endoplasmic reticulum (ER) and fluxes mostly generated by the membrane pumps compensating Ca^{2+} leaks across the plasma and ER membranes. IP_3 is synthesised by Ca^{2+}-dependent and G protein-dependent phospholipase C (PLC). IP_3 concentration also has a major impact on the Ca^{2+}-dependent inositol triphosphate receptor (IP_3R) located on the ER membrane.

The network responsible for Ca^{2+} oscillations in *Dictyostelium* constitutes two feedback mechanisms. The first feedback loop is based on the movement of Ca^{2+} ions between the ER and cytoplasm. Intracellular Ca^{2+} is sequestered into the ER by Sarco/Endoplasmic Reticuluum Ca^{2+}-ATPase (SERCA). It is released from the ER back into the cytoplasm *via* the IP_3R (which has both a Ca^{2+} and IP_3 dependence[38]), as well as by a direct leak through the ER membrane. Another feedback mechanism involves the Ca^{2+} release from the intracellular compartment into the extracellular space by a plasma membrane Ca^{2+} pump (PMCA). PMCA compensates for the constant Ca^{2+} leak throughout the surface of the plasma membrane into the intracellular space. Other routes of Ca^{2+} into the cytoplasm include a range of Ca^{2+} channels, including the stretch-activated Ca^{2+} channels which play a particularly important role in *Dictyostelium* chemotaxis[39] *via* the directed migration mechanism.[40,41] IP_3 is produced by the only PLC isoform found in *Dictyostelium* which is structurally similar to the mammalian PLCδ isoform and regulated by both Ca^{2+} and G-protein pathways.[42–44] IP_3 is further converted into IP_4 by IP_3 kinase (IP_3K).

The intracellular Ca^{2+} regulation network described above is directly connected in our model with the G protein coupled pathways included in some previously published models.[10,22,23] Intracellular cAMP in *Dictyostelium* can be produced by ACA, ACB and ACG adenylate cyclase isoforms. ACA is related to the mammalian and Drosophila G protein-coupled adenylyl cyclases, reported to be expressed during aggregation.[45] This isoform is responsible for the synthesis of cAMP in early development and plays a role in cell-cell signalling. The other two isoforms, ACB and ACG, are involved in terminal differentiation and spore germination, respectively. Given the focus of this study on elucidating the molecular mechanisms controlling cellular aggregation, our model includes the ACA isoform only. Since the (direct or indirect) dependence of ACA on the G-protein and Ca^{2+} pathways in *Dictyostelium* has not been as completely characterized experimentally as in the case of some mammalian adenylyl cyclases, we computationally tested a number of different mechanisms for the ACA activation and chose the one that led to stable robust oscillations displaying the correct relationship between the Ca^{2+} and cAMP waveforms. In the model, the cAMP release from the cell incorporates two Ca^{2+} and cAMP-dependent terms. The released cAMP diffuses in all directions and influences both the cell that pumped it, and any surrounding cells present in the vicinity. It is also degraded by extracellular PDE which is released with cAMP and by a PDE isoform expressed on the surface of *Dictyostelium*. The cAMP-cAR1 interactions lead to ACA, ERK2 and PLC activation *via* the G-protein pathways. ERK2 when activated through the cAR1 G protein-coupled pathway can inhibit RegA activity and at the same time stimulate ACA. PKA phosphorylates and thereby inhibits ERK2 and cAR1 in a cAMP-dependent manner.

The complete set of equations making up the proposed model are presented in the Methods section of the paper. Fig. 2 shows the stable oscillations of Ca^{2+}, cAMP and enzyme activities predicted by the numerical solutions of these equations. The period, frequency and phase relations of the

View Online

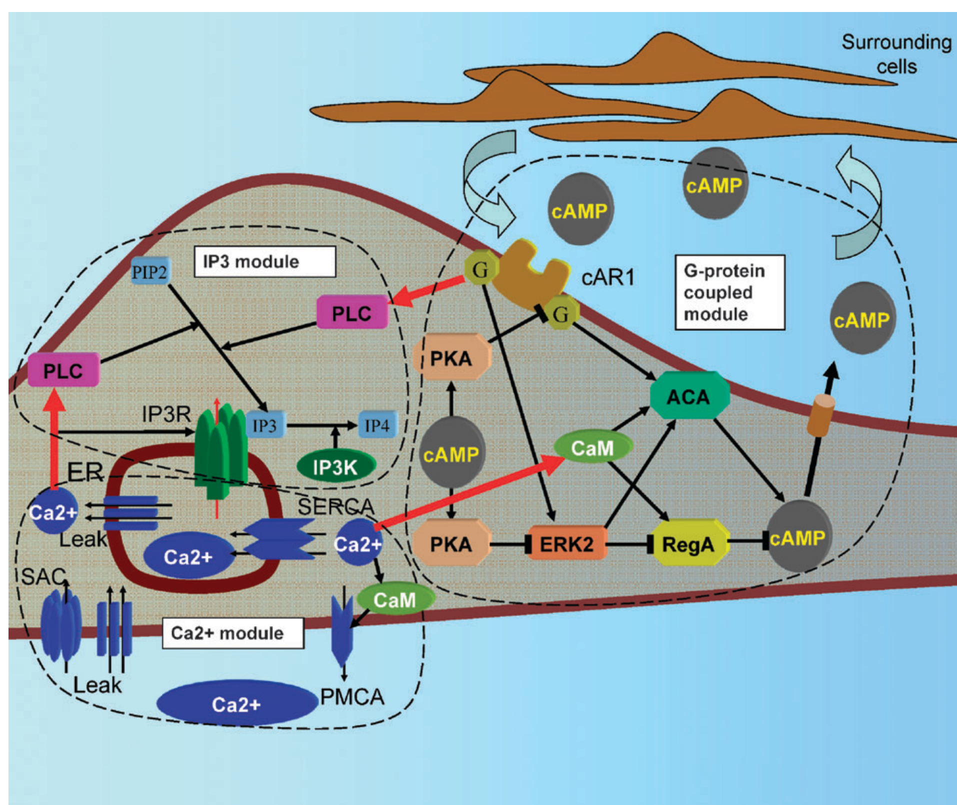

Fig. 1 The three modules, and their interconnections (shown in red), included in our model for cAMP oscillations in *Dictyostelium*. As shown schematically in the figure, there is a close interdependence between the Ca^{2+}, IP_3 and G protein-coupled modules included in our model. $cAMP_i$ is produced by ACA and hydrolyzed by PDE in a Ca^{2+}-CaM dependent manner. Ca^{2+} is regulated by a number of proteins including IP_3 channels and Ca^{2+} pumps on both basal and ER membranes. Release of $cAMP_e$ and the subsequent cAR1 interactions lead to the cyclic alterations of $cAMP_i$, $cAMP_e$, Ca^{2+} and IP_3 concentrations. IP_3 is synthesized by PLC in response to $cAMP_e$ dependent cAR1 activation and recycled further by IP_3 specific kinases and phophatases. Extracellular cAMP binding to cAR1 activates ERK2, PLC and ACA *via* the G-protein subunits. $cAMP_i$ produced by ACA activates PKA which phosphorylates and thereby inhibits ERK2 as well as ACA *via* the cAR1/G-protein pathway. Connecting intermediates are not included in this diagram; the arrows shown represent both direct and indirect interactions.

oscillations in the modelled variables all show good agreement with experimentally observed results. The amplitude of predicted Ca^{2+} oscillations is in the physiological range of several hundreds of nM.[46] The period of predicted oscillations is of the order of 6–7 min which also corresponds closely to the experimentally observed values.[22,23] The relationship between the phases of the Ca^{2+} and cAMP oscillations is defined by the properties of ACA. It has been shown previously that Ca^{2+}-CaM-dependent protein regulation is dependent on the number of Ca^{2+} ions bound to CaM[47] and the complex interplay between the Ca^{2+} and G-protein pathways thus leads to a diversity of cAMP activation patterns.[48] We computationally elucidated three possibilities (Fig. 3) for hypothetical direct or indirect ACA activation by CaM in complex with zero (Fig. 3A), one (Fig. 3B) and two (Fig. 3C) Ca^{2+} ions, leading to three potential scenarios for the interplay between Ca^{2+} and G-protein signals. In one case (Fig. 3A) Ca^{2+} inhibits the ACA activity and any activation by G-protein coupled receptors is only possible when there is no Ca^{2+} signal. If ACA is regulated by Ca^{2+}-CaM complexes with one or two Ca^{2+} ions bound to CaM however, (Fig. 3B and C, respectively), the dependence on Ca^{2+} becomes bell shaped with an "optimal" Ca^{2+} concentration. In these cases, any signal from the G-protein pathways further amplifies the ACA activity. The mechanism for ACA activation shown in Fig. 3C has been used in our model, since it corresponds to the most likely situation corresponding to the correct phase relationship between the cAMP and Ca^{2+} oscillations.

We note three distinct situations on the graph shown in Fig. 3C, labelled as cases 1, 2 and 3. When Ca^{2+} is very low (case 1) or very high (case 3) the system largely depends on the G-protein pathway only, in a sigmoid dependent manner. In the intermediate Ca^{2+} concentrations, the G-protein signalling is magnified, the sigmoid type-dependence on G-pathway signals is still present, but there is a strong signal even in response to a low G-protein pathway incoming dynamics. The ACA dependence on Ca^{2+}, as can be seen from the ACA *versus* Ca^{2+} projection without considering the G-protein signals, represents a bell shaped curve, which leads to the full ACA activation in the intermediate intracellular Ca^{2+} concentration range and inhibition at high and low Ca^{2+} levels. An in-depth analysis of the Ca^{2+} and G-protein cross-talk mechanisms is presented in ref. 48. The Erk2

 This journal is © The Royal Society of Chemistry 2009

Published on 16 April 2009 on http://pubs.rsc.org | doi:10.1039/B822074C
Downloaded by University of Northumbria on 15 October 2012

View Online

Downloaded by University of Northumbria on 15 October 2012
Published on 16 April 2009 on http://pubs.rsc.org | doi:10.1039/B822074C

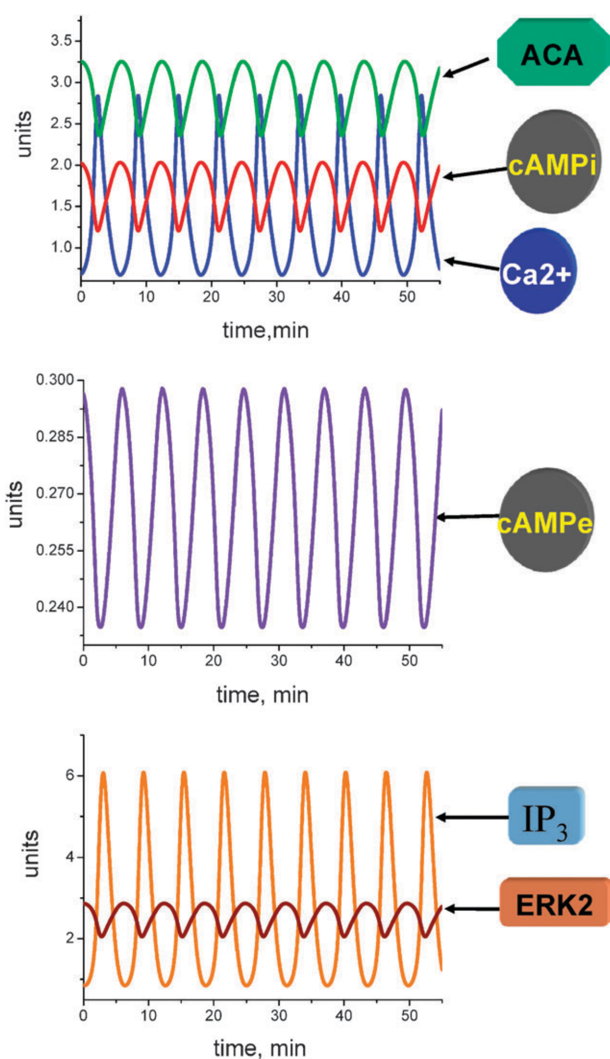

Fig. 2 The steady-state oscillations in *Dictyostelium*. The time evolution of enzymatic activities as well as intracellular cAMP, IP_3 and Ca^{2+} generated by numerical solution of the model equations. Units are concentrations of activated enzyme (μM). The model displays stable oscillations with periods, amplitudes and phase relationships among all key variables showing a good match to experimental data.

dependence is not shown on this graph, as it is incorporated in the model by utilising the law of mass action reaction as described in the Methods section. The ACA regulation is undoubtedly one of the key mechanisms participating in the interplay of the three modules considered in this manuscript. The computational results shown in Fig. 3C provide an example of how experimental data (summarized in Fig. 1) may be augmented by Systems Biology analysis to provide new interpretations which are not obvious from a straightforward analysis of the biological circuit diagram.

We next investigated the ability of the proposed model to replicate the experimentally observed levels of entrainment between separate oscillating *Dictyostelium* cells. Specifically, we were interested in the relationship between the oscillations of intracellular cAMP in one cell and the alterations of extracellular cAMP concentration caused by multiple surrounding cells. Fig. 4 shows the effects in our model of synchronization between the extracellular oscillations mediated by a number of cells and the oscillations initiated independently by a single *Dictyostelium* cell. It is clear from Fig. 4A that the extracellular cAMP alterations, even when applied at different time points (data not shown) with respect to the internal oscillations, have a modulatory effect on a cell, and quickly achieve absolute synchronization. In other words, external oscillations of higher amplitude can always entrain the oscillations in an individual cell regardless of the initial differences in phase. As expected, reducing the amplitude of cAMP oscillations in the extracellular medium results in a corresponding reduction in the level of entrainment (Fig. 4B), while the ability of external cAMP oscillations to change the frequency of the oscillations within a single cell is clearly shown in Fig. 4C and D.

The proposed model provides a mechanistic explanation of the experimentally observed effects of calmidazolium on cytostolic free Ca^{2+} concentration

It has been shown experimentally that the wavelike pulses of cAMP released in suspensions of *Dictyostelium* cells are coupled with oscillations of light scattering.[39,49] The oscillations of light scattering, in turn, have been reported to depend on Ca^{2+} mechanisms,[50] including the release and re-uptake of Ca^{2+} from the intracellular compartment into the extracellular space, and feedback loops between the intracellular compartment and intracellular Ca^{2+} stores.[33,51–54] In order to investigate the above issues quantitatively, we included the networks regulating the Ca^{2+} flows through the extracellular space, intracellular compartment and ER in the proposed mathematical model. We also incorporated a simple dependence of the cell shape alterations on the intracellular Ca^{2+} concentration. We then used the model to provide a mechanistic interpretation of the results of experiments with the application of the CaM inhibitor, calmidazolium (R24571), which causes a transient surge in cytosolic free Ca^{2+} concentration.[26,28]

It has been shown that one of the targets for the R24571 action is the CaM that regulates PMCA.[55,56] PMCA pumps Ca^{2+} out of the cytoplasm and compensates for the constant Ca^{2+} leak through the plasma membrane. In order to evaluate the action of calmidazolium, we incorporated two potential time courses of the compound action on the CaM activity (Fig. 5A). In one case, CaM activity was inhibited and subsequently kept at that level. In this case, the model predicted the disappearance of cellular oscillations (Scenario 1 in Fig. 5A). In another scenario, the effect of R24571 on CaM activity was modelled as a temporary inhibition, with a subsequent complete recovery in the level of CaM activity. Under this assumption, the application of calmidazolium caused a surge of Ca^{2+}, after which the oscillations returned to their previous levels (Scenario 2 in Fig. 5A). At the same time the temporal Ca^{2+} surge is observed in both scenarios. Since this second response is consistent with the R24571 application experiments, the results of our computational analysis lead us suggest that CaM is

View Online

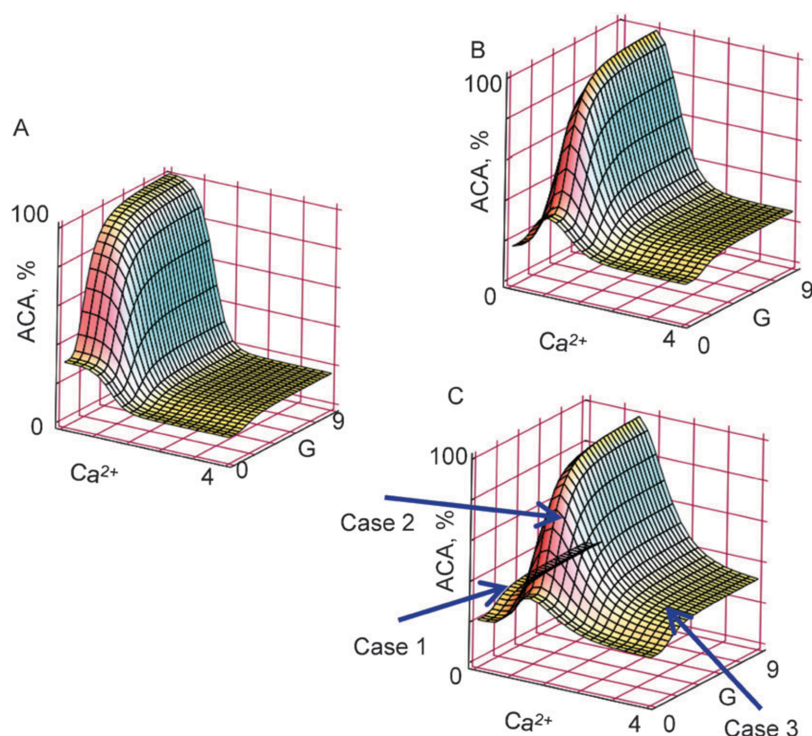

Fig. 3 ACA activity dependence on the Ca^{2+} and G-protein mediated signals. The dependence of ACA activity (as a percentage of full activation) is shown according to the following assumptions: (A) ACA is regulated by CaM in the apo-state, (B) ACA depends on CaM with one Ca^{2+} ion bound and (C) ACA is governed by CaM in complex with two bound ions of Ca^{2+}. The last possibility has been employed in the present model as being the most realistic case in the light of recent structural studies. The three situations discussed in the text are denoted as cases 1, 2 and 3 in the Figure.

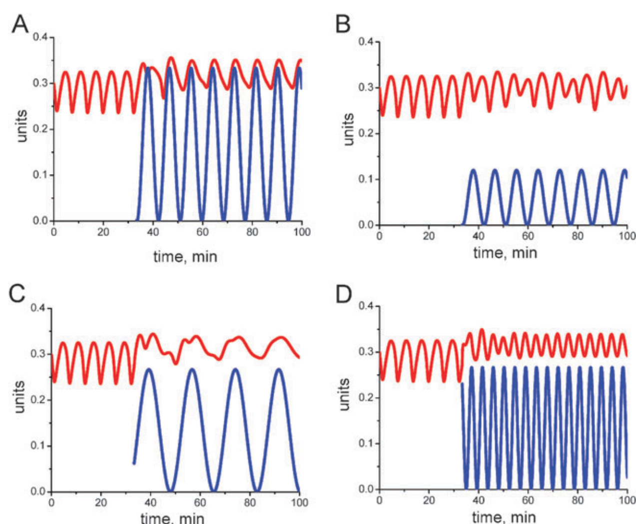

Fig. 4 Entrainment of an individual *Dictyostelium* cell by surrounding cells in our model. (A) The extracellular cAMP oscillations generated by aggregating *Dictyostelium* cells cause an individual cell to oscillate with the same phase even when the extracellular oscillations are applied at a random time point in the oscillatory cycle. (B) Extracellular cAMP oscillations of smaller amplitude have a lesser effect on an individual cell. (C) and (D) Extracellular cAMP oscillations of variable frequency entrain oscillations of a single *Dictyostelium* cell.

inhibited temporally (Fig. 5B) and that the Ca^{2+}-CaM-dependent regulation of PMCA appears to be one of the main targets for calmidazolium action in the light scattering experiments.[26,57] More generally, the precise nature of the relationship between cellular oscillations of cAMP, Ca^{2+} and other intracellular enzymatic activities in an individual *Dictyostelium* cell and the oscillations of optical density observed in a number of cells remains somewhat unclear. The changes in optical density may be due to either an increased number of cells or to cell shape alterations. Both these factors depend on the lamellipodia formation and disassembly turnover as cells migrate during aggregation. Amongst many other factors, intracellular Ca^{2+} has been shown to modulate both the speed and direction of *Dictyostelium* motility.[1] In an attempt to shed light on the above issues, we employed our model to develop the following testable hypothesis. We sought to investigate whether or not the Ca^{2+} surges caused by the application of calmidazolium added at different time points of the oscillatory cycle would result in similar phase delays in optical density oscillations to those observed experimentally in ref. 26. Fig. 5C shows the various perturbations caused to the oscillations of intracellular Ca^{2+} by application of R24571 at different time points of the oscillatory cycle. The corresponding normalized phase shifts, as a function of the time point of the R24571 application, are shown on Fig. 5D. The strong agreement between these values and the experimental data points in the phase diagram depicting the magnitude of the phase shifts induced by R24571 reported in ref. 26 reinforces the notion that strong interactions between Ca^{2+} and cAMP oscillations, as specified in our model, are crucial to the regulation of *Dictyostelium* migration during aggregation.

Downloaded by University of Northumbria on 15 October 2012
Published on 16 April 2009 on http://pubs.rsc.org | doi:10.1039/B822074C

 This journal is © The Royal Society of Chemistry 2009

View Online

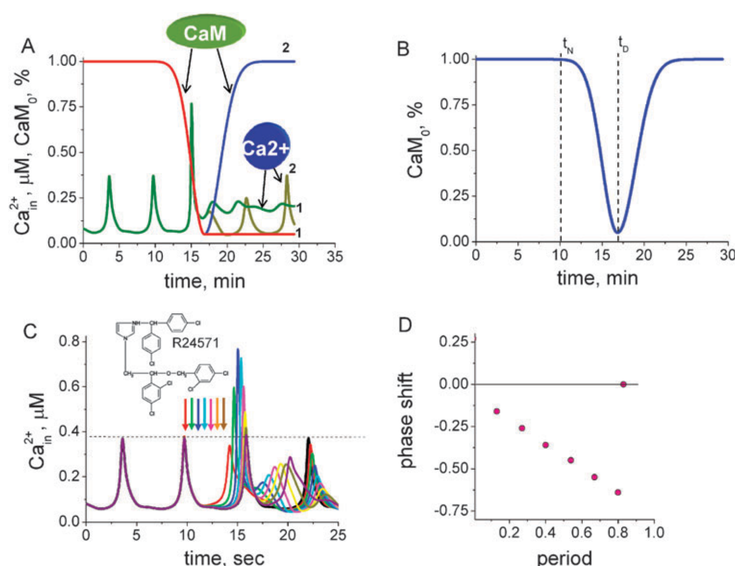

Fig. 5 Model predictions for the effect of calmidazolium (R24571) on light scattering during *Dictyostelium* aggregation. (A) Two theoretical CaM inhibition effects caused by R24571 are shown. In one case CaM activity has been inhibited and subsequently kept at a low level (red line, 1). The model predicts that this type of inhibition abolishes cellular oscillations (green line 1). In a different scenario, CaM activity is temporarily inhibited by calmidazolium and then returns to its initial level (blue line 2). In this case, the Ca^{2+} oscillations return to their normal levels after a transition phase (olive line, 2). The latter case is more consistent with the experimental observations.[26,28] (B) CaM inhibition profile employed in the present model. t_N and t_D denote the time frame of calmidazolium application. (C) The effects of R24571 addition at different time points of the oscillatory cycle (shown as multiple arrows) on the intracellular Ca^{2+} oscillations. The dotted line shows a threshold above which the Ca^{2+} surges are assumed to influence lamella formation and thereby have an impact on the optical density in aggregation. (D) Predicted phase shifts are plotted against the time point of R24571 addition within an oscillatory cycle. The duration of a phase (the time between the peaks of spikes) was normalized to 1. The predicted phase shifts' dependence on the calmidazolium application time points show good agreement with the experimental data provided in ref. 26.

Downloaded by University of Northumbria on 15 October 2012
Published on 16 April 2009 on http://pubs.rsc.org | doi:10.1039/B822074C

The proposed model highlights the role of stretch-activated Ca^{2+} channels and extracellular PDE in *Dictyostelium* aggregation

The two key factors characterizing cell motion during *Dictyostelium* aggregation are the direction and velocity of migration.[39] It has been shown that in the absence of an extracellular cAMP gradient, *Dictyostelium* cells undergo a random motion, while they will move up the cAMP gradient when it exists. We employed the proposed model in order to seek new insights into the potential relationship between the cellular oscillations in *Dictyostelium* and migration in chemotaxis by varying two critical extracellular parameters which are very likely to influence cellular oscillations.

First we varied the level of extracellular PDE, because it is released together with cAMP during the periodic oscillations and has a strong influence on the extracellular feedback loop. Recent experimental results have also shown that a PDE isoform is expressed on the outer surface of the *Dictyostelium* cell membrane.[58] Fig. 6A reveals the emergence followed by the disappearance of ACA oscillations predicted by our model in response to a gradual increase and decrease in the extracellular PDE concentration (Fig. 6B). The observed pattern of oscillations closely matches the experimentally measured periodic oscillations in *Dictyostelium* that have been shown to spontaneously appear during development.[22]

A second factor that was investigated using the proposed model was the overall conductivity of SACs, which have been shown to be one of the major players in governing cell

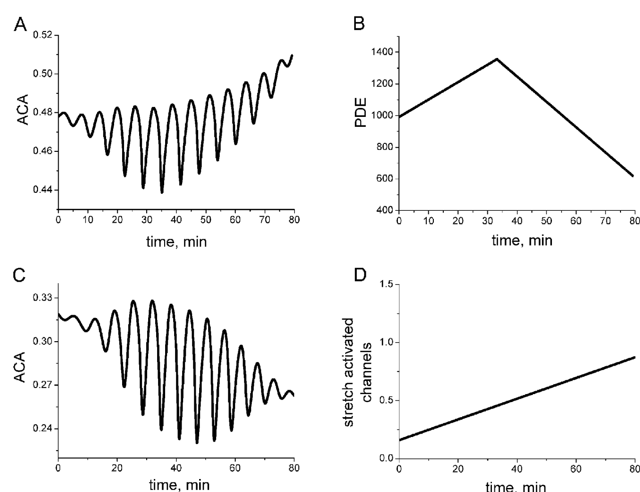

Fig. 6 The role of extracellular PDE and stretch-activated Ca^{2+} channels in maintaining cellular oscillations. The figure shows model predictions for the impact of two crucial parameters for cell migration on the cellular oscillations in *Dictyostelium*. ACA oscillations (A) and (C) are shown as a function of the extracellular PDE activity (B) and overall conductance of stretch-activated Ca^{2+} channels (D). The lines showing the extracellular PDE activity (B) and overall conductance of stretch-activated Ca^{2+} channels (D) represent the hypothetical PDE activity and SACs conductivity levels that can be controlled by of the intracellular PDE and extracellular SACs inhibitors, respectively. Variations of both stretch-activated Ca^{2+} channels (D) and extracellular PDE (B) predict that oscillations can exist only within the physiological domain shown.

View Online

Downloaded by University of Northumbria on 15 October 2012
Published on 16 April 2009 on http://pubs.rsc.org | doi:10.1039/B822074C

migration.[41] Since during migration all cells undergo membrane protrusion and retraction cycles, stretch-activated Ca^{2+} channels inevitably play a role in chemotaxis *via* the intracellular Ca^{2+} circuit. Fig. 6C reveals the emergence followed by the disappearance of ACA oscillations predicted by our model in response to a linear elevation of the number of SACs in the open state (Fig. 6D).

The above model predictions that the existence of stable oscillations depends on two "migration"-specific parameters, together with the corresponding experimental results now available in the literature, lead us to propose a central role for the intracellular Ca^{2+} circuit in ensuring chemotaxis-dependent aggregation in *Dictyostelium*. According to previous studies, intracellular Ca^{2+} oscillations are required for the turnover of focal adhesions (FA)s in migrating cells.[40,59] It has also been reported that the Ca^{2+} concentration is lower in the leading lamellipodia[60,61] of migrating cells. Taken together, these results lead us to suggest that Ca^{2+} plays a role not only in the locomotion mechanism, but also in defining the direction of migration. The Ca^{2+} network in *Dictyostelium* appears to be complementary to the G protein-coupled cAMP network, and their oscillations observed in aggregation appear to be the core cellular engine allowing movement in the direction defined by extracellular conditions such as cAMP gradient and the presence of nutrition. While the alterations in extracellular cAMP concentrations provide the external cues which guide the direction of migration, our model underlines the important role of Ca^{2+} in actually achieving directionality of motion. By protruding more lamella on one side of the cell and retracting it on the other, the intracellular machinery thus carries out the routine job of membrane protrusion according to the extracellular stimuli, focal adhesion assembly, tail retraction and focal adhesion disassembly in an intracellular Ca^{2+} and cAMP oscillation-dependent manner.

Interactions between calcium, IP_3 and G protein-dependent networks significantly improve the robustness of cAMP oscillations

At the very beginning of the aggregation process, some spatially isolated *Dictyostelium* cells are able to independently generate stable oscillations in their levels of intracellular cAMP, even in the absence of strong extracellular cAMP waves. Previous computational studies have suggested that the release of cAMP by an individual cell with subsequent binding of some portion of extracellular cAMP to the cAR1 receptor constitutes the key feedback mechanism required for maintaining stable cAMP oscillations during this phase of the aggregation process.[23,62] Although initial robustness analysis studies of the models proposed for this feedback loop showed it to be surprisingly fragile, with rather small variations in the system's kinetics destabilising the resulting cAMP oscillations,[23,62] subsequent analyses taking into account the effects of stochastic noise and extracellular synchronisation showed improved levels of robustness.[23,62] In this section, we show that dynamic interactions between (apparently redundant) Ca^{2+}, IP_3 and G protein-dependent modules included in our model have the effect of further significantly improving the robustness of the overall system, allowing the maintenance of stable cAMP oscillations for an individual cell even in the absence of strong extracellular cAMP waves.

To quantify the effect of these interactions on the robustness of the generated cAMP oscillations, we compared the robustness properties of the proposed model with those of a

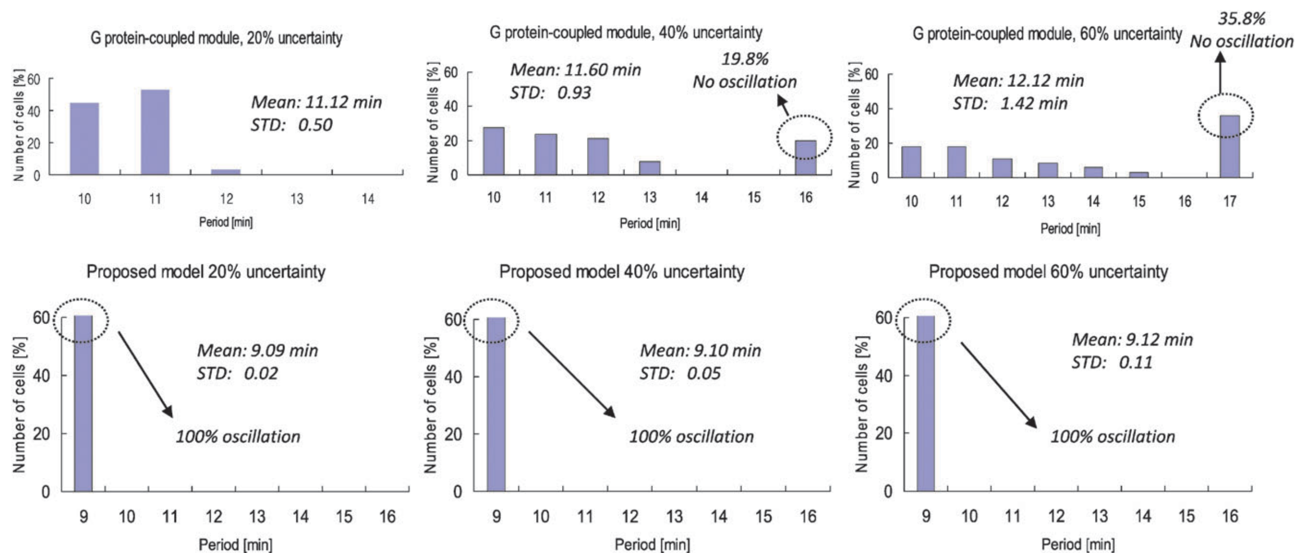

Fig. 7 Robustness analysis of the period of the internal cAMP oscillations with respect to perturbations in model parameters. The figure shows the period distribution of the model including the G protein-coupled module only (first row) and the proposed model (second row) for one cell with 20%, 40%, and 60% perturbations in the four kinetic parameters determining the dynamics of the extracellular cAMP positive feedback loop. The bar on the extreme right represents the percentage of cells that are not oscillating. As the size of the perturbation increases, the proportion of non-oscillating cells increases from 0% to 32% for the model incorporating the G protein-coupled module only, whereas in the proposed model all cells display stable oscillations for all perturbations considered. The standard deviations of the periods are more than an order of magnitude smaller for the proposed model, even though the standard deviation is calculated only for the cells displaying stable oscillations in each case. Each plot is the result of 1000 simulations for different random samples of the model parameters using a uniform distribution about the nominal values.

 This journal is © The Royal Society of Chemistry 2009

View Online

Downloaded by University of Northumbria on 15 October 2012
Published on 16 April 2009 on http://pubs.rsc.org | doi:10.1039/B822074C

previous model for cAMP oscillations which included only the G protein-dependent module.[23,62] We generated 1000 random samples of the 4 kinetic constants governing the dynamics of the extracellular cAMP feedback loop in each model from uniform distributions around the nominal values, for several different uncertainty ranges (see Methods). The period distributions of each model for three levels of uncertainty in the kinetic parameters, *i.e.*, 20%, 40%, and 60%, are shown in Fig. 7. In the figures, the bar on the extreme right denotes the total number of cases where stable oscillations were not observed and the trajectories converged to some steady state value. Note that the proportion of non-oscillatory trajectories is 23% and 32% for the G protein-coupled receptor model with a 40% and 60% level of uncertainty, respectively, while for the proposed model all cells continued to display stable oscillations even for the highest level of parameter uncertainty. Also, the standard deviation of the periods is more than an order of magnitude smaller for the proposed model, even though the standard deviation is calculated only for the cells displaying stable oscillations in each case.

Similar improvements in the robustness of the amplitude distributions are shown in Fig. 8—note that although the standard deviations of the amplitudes appear to be similar for both models, in reality there is a much greater level of variation in the amplitudes of the G protein-coupled module. This is because the standard deviations are calculated only for those cells displaying stable oscillations in each case, and it is precisely those cells which are no longer generating stable

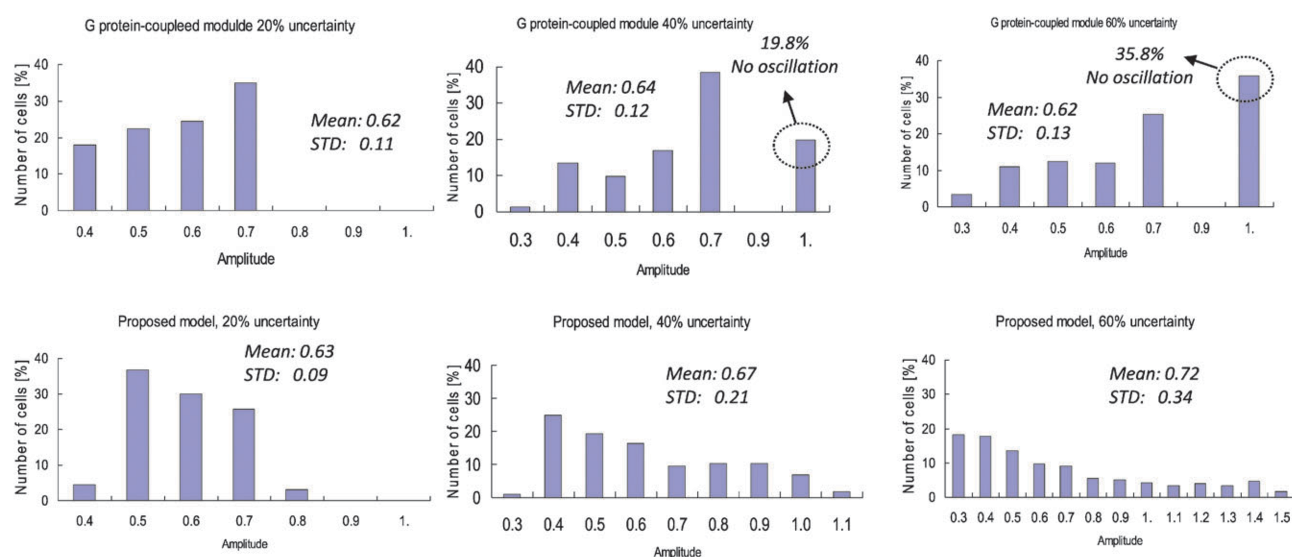

Fig. 8 Robustness analysis of the amplitude of the internal cAMP oscillations with respect to perturbations in model parameters. The figure shows the amplitude distribution of the model including the G protein-coupled module only (first row) and the proposed model (second row) for one cell with 20%, 40%, and 60% perturbations in the four kinetic parameters determining the dynamics of the extracellular cAMP positive feedback loop. The bar on the extreme right represents the percentage of cells that are not oscillating. As the size of the perturbation increases, the proportion of non-oscillating cells increases from 0% to 32% for the model incorporating the G protein-coupled module only, whereas in the proposed model all cells display stable oscillations for all perturbations considered. Note that although the standard deviations of the amplitudes appear to be similar for both models, this does not accurately reflect the greater level of variation in the dynamics of the G protein-coupled module, as the standard deviations are calculated only for those cells displaying stable oscillations in each case. Each plot is the result of 1000 simulations for different random samples of the model parameters using a uniform distribution about the nominal values.

Table 1 Robustness analysis comparison

	Laub Loomis model		Proposed model	
	Period/min	Amplitude	Period/min	Amplitude
20% perturbation	Mean: 11.12 STD: 0.50	Mean: 0.62 STD: 0.11	Mean: 09.09 STD: 0.02	Mean: 0.63 STD: 0.09
40% perturbation	Mean: 11.60 STD: 0.93 19.8% no oscillation	Mean: 0.64 STD: 0.12	Mean: 9.10 STD: 0.05	Mean: 0.67 STD: 0.21
60% perturbation	Mean: 12.12 STD: 1.42 35.8% no oscillation	Mean: 0.62 STD: 0.13	Mean: 9.12 STD: 0.11	Mean: 0.72 STD: 0.34
80% perturbation	Mean: 12.08 STD: 1.38 51.2% no oscillation	Mean: 0.62 STD: 0.13	Mean: 9.26 STD: 0.94	Mean: 0.73 STD: 0.45

View Online

cAMP oscillations which have the largest deviation from the nominal amplitude values. A summary of the robustness analysis comparisons with 20%, 40%, 60% (and 80%) perturbations is given in Table 1.

Discussion

This study presents a new computational model which balances a number of pieces of recent experimental data in an attempt to link molecular interactions at the cellular level with *Dictyostelium* behaviour during aggregation *via* chemotaxis. The mathematical model developed for this purpose incorporates the three major modules which are known to govern the relevant cellular events, and allows a direct quantitative analysis of how intracellular Ca^{2+} interacts with cAMP oscillations in *Dictyostelium*. In previous studies these modules have been modelled and analysed separately, however, recent experimental evidence suggests strong interactions between them, highlighting the need for an integrated model. The key coupling points between the networks include ACA and RegA that synthesize and hydrolyze intracellular cAMP, respectively. Another crucial piece of experimental evidence comes from the application of CaM blockers leading to the inhibition of light scattering oscillations during aggregation. Our model, which incorporates both cAMP and Ca^{2+} alterations, predicts intracellular and extracellular cAMP oscillations which are similar to those generated by previous models for cAMP regulation in *Dictyostelium*. However, unlike these models, it allows us to directly investigate how Ca^{2+} perturbations lead to cAMP-dependent effects. The proposed model also suggests a potential mechanism for Ca^{2+}-dependent *Dictyostelium* migration, modulated by external cAMP waves during aggregation.

Under unfavourable environmental conditions, *Dictyostelium* cells start releasing extracellular cAMP and an area containing several cells becomes the centre of attraction to other cells. However, no aggregation would be possible if cells could not migrate up the cAMP gradient. Our model suggests that the intracellular Ca^{2+} network plays a key role in generating the internal motor for cell locomotion. Indeed, given that Ca^{2+} concentration alterations, observed in migrating cells,[63,64] can be a key factor in FA disassembly,[65,66] as well as the finding that lamellae formation is inversely proportional to cAMP concentration,[67] it seems reasonable to propose the direct involvement of both the Ca^{2+} and cAMP networks in migration *via* the lamella protrusion and retraction mechanisms.

Although the extracellular cAMP feedback loop *via* cAR1 clearly plays an important role in generating cAMP oscillations, it is also somewhat surprising that such a loop can be maintained robustly solely by the self-release of cAMP by the same cell, as the amount of cAMP released in this manner is likely to be very small, and the diffusion and degradation mechanisms are likely to further diminish even that amount. In the light of our analysis, it seems reasonable to propose that in certain situations, a complementary oscillator functioning *via* the Ca^{2+}-regulating proteins may initiate intracellular Ca^{2+} alterations, and in turn, cAMP oscillations, when necessary. However, the Ca^{2+} network is itself highly complex and is regulated by multiple mechanisms, including extracellular cAMP *via* the cAR1 receptor and the SACs located on the extracellular membrane. Our results suggest that all of these factors are crucial for the generation of oscillations. The necessity of both intracellular Ca^{2+} and cAMP oscillations for *Dyctiostelium* migration during aggregation is supported by the model predictions for the application of CaM blocker. The inhibition by the CaM blocker of light scattering oscillations, modelled based on the assumption that filopodia and lamellipoda are being assembled and disassembled in a Ca^{2+} dependent manner, lends further supports to the necessity of Ca^{2+} oscillations in *Dictyostelium* aggregation. Indeed, a range of experimental reports from other types of cells confirm the role of Ca^{2+} as an intracellular engine for cellular locomotion. Ca^{2+} oscillations were observed in migrating neutrophils (See Fig. 1 of ref. 63) and were absent when cells were stationary. Chemotaxis studies in newt eosinophils[60,61] revealed that there is less Ca^{2+} in the front than in the rear of migrating cells, while a detailed analysis of Ca^{2+} involvement in the direction and the speed of migration *via* the alteration of the cellular shape and FA adhesion dynamics as a function of various oscillation regimes is shown in ref. 40.

Conclusions

It has recently been argued that an important property that engineering and biological systems appear to have in common is the need for rather elaborate functional design strategies in order to generate robustly operational systems—while minimal designs are sufficient to generate nominal functionality, they often fail to provide crucial aspects of robustness and performance necessary for competitive survival in challenging environments. Examples of the use of complex designs to increase system robustness are abundant in the technological sciences, while examples from the natural sciences are still emerging. In the case of the system considered here, it appears that synchronisation effects between the different intracellular modules have a beneficial effect on overall systems robustness, a result which is consistent with our previous study of synchronisation effects between different *Dictyostelium* cells *via* the diffusion of external cAMP.[68] The results of our analysis clearly show the improved robustness which is achieved in *Dictyostelium* cells by employing three coupled functional modules to generate cAMP oscillations, instead of a single network based on the G protein-coupled receptor pathway, and thus provide another concrete biological example of this type of "elaborate robust" design strategy.

Methods

The model equations

This model is designed to simulate and analyze the cAMP, Ca^{2+} and IP_3 oscillations in an individual *Dictyostelium* cell when it is interacting with surrounding cells *via* extracellular cAMP. As shown in Fig. 1, the model has a modular structure, incorporating Ca^{2+}, IP_3 and G protein-coupled modules and the interactions between them. The time courses of the model

Downloaded by University of Northumbria on 15 October 2012
Published on 16 April 2009 on http://pubs.rsc.org | doi:10.1039/B822074C

 This journal is © The Royal Society of Chemistry 2009

Downloaded by University of Northumbria on 15 October 2012
Published on 16 April 2009 on http://pubs.rsc.org | doi:10.1039/B822074C

components are presented as a system of ordinary differential equations:

$$
\begin{aligned}
&(V_i - V_{\mathrm{ER}})\cdot\frac{\mathrm{d}[\mathrm{Ca}_i^{2+}]}{\mathrm{d}t} = (S_i\cdot(J_i^{\mathrm{in}} - J_i^{\mathrm{out}}) + S_{\mathrm{ER}}\cdot(J_{\mathrm{ER}}^{\mathrm{out}} - J_{\mathrm{ER}}^{\mathrm{in}})),\\
&V_{\mathrm{ER}}\cdot\frac{\mathrm{d}[\mathrm{Ca}_{ER}^{2+}]}{\mathrm{d}t} = S_{\mathrm{ER}}\cdot(J_{\mathrm{ER}}^{\mathrm{in}} - J_{\mathrm{ER}}^{\mathrm{out}}),\\
&(V_i - V_{\mathrm{ER}})\cdot\frac{\mathrm{d}[\mathrm{IP}_3]}{\mathrm{d}t} = ((r_0 + r_1)\cdot S_i\cdot N_{\mathrm{PLC}}\cdot p_{\mathrm{PLC}})\cdot S_i\cdot[\mathrm{PIP}_2] - r_2\cdot\mathrm{IP}_3K,\\
&V_i\cdot\frac{\mathrm{d}(\mathrm{cAMP}_i)}{\mathrm{d}t} = k_1\cdot\mathrm{ACA} - k_2\cdot\mathrm{RegA}\cdot\frac{\mathrm{cAMP}_i}{k_{\mathrm{RegA}} + \mathrm{cAMP}_i},\\
&V_e\cdot\frac{\mathrm{d}(\mathrm{cAMP}_e)}{\mathrm{d}t} = S_i\cdot J_{\mathrm{cAMP}i} + S_m\cdot J_{\mathrm{cAMP}e} - k_3\cdot\mathrm{PDE}_e\cdot\frac{\mathrm{cAMP}_e}{k_{\mathrm{PDE}} + \mathrm{cAMP}_e},\\
&V_i\cdot\frac{\mathrm{dERK2}}{\mathrm{d}t} = -n_1\cdot\mathrm{ERK2}\cdot\mathrm{Phos} + n_2\cdot(\mathrm{ERK2}_0 - \mathrm{ERK2})\cdot\mathrm{PKA},\\
&V_i\cdot\frac{\mathrm{dACA}}{\mathrm{d}t} = -l_1\cdot\mathrm{ACA}\cdot\mathrm{Phos} + l_2\cdot(\mathrm{ACA}_0 - \mathrm{ACA})\cdot\mathrm{PKA}.
\end{aligned}
\tag{1}
$$

where V_i and V_{ER} are the cytoplasmic and ER volumes, respectively. $[\mathrm{Ca}^{2+}]_i$ (mol l^{-1}) is the free Ca^{2+} concentration in the intracellular volume ($V_i - V_{\mathrm{ER}}$). $[\mathrm{Ca}^{2+}]_{\mathrm{ER}}$ is the free Ca^{2+} in the ER volume V_{ER}. J_i^{in} and J_i^{out} (mol sec^{-1} $\mu\mathrm{m}^{-2}$) are the Ca^{2+} ion flows through the cytoplasmic membrane into the cytoplasm and out into the extracellular space, respectively. $J_{\mathrm{ER}}^{\mathrm{in}}$ and $J_{\mathrm{ER}}^{\mathrm{out}}$represent the flow of Ca^{2+} ions through the ER membrane into the ER and out into the cytoplasm, respectively. S_i, S_{ER} ($\mu\mathrm{m}^2$) are the surface areas of the cytoplasmic and ER membranes. r_0 (sec^{-1}) and r_1 (sec^{-1}) are the PIP_2 hydrolysis rates by PLC, that reflect G-protein and Ca^{2+}-dependent pathway activation, respectively, r_2 (sec^{-1}) is an average IP_3 conversion rate by $\mathrm{IP}_3\mathrm{K}$ into IP_4, N_{PLC} ($\mu\mathrm{m}^{-2}$) is a number of PLCs per $\mu\mathrm{m}^2$, and p_{PLC} is the probability of PLCs being in the active form. cAMP_i (mol l^{-1}) is the free cAMP concentration in the intracellular volume ($V_i - V_{\mathrm{ER}}$), *ACA* is the concentration of the intracellular ACA, which in turn depends on the intracellular Ca^{2+} concentration, extracellular cAMP_e *via* the cAR1 and G-proteins, and on the intracellular cAMP_i concentration *via* phosphorylation by cAMP-dependent PKA. RegA is the intracellular phosphodiesterase that hydrolyses intracellular cAMP. k_1 (sec^{-1}) is the ACA enzymatic activity rate, k_2 (sec^{-1}) is the enzymatic RegA activity rate, and k_{RegA} (mol) is the cAMP-RegA dissociation constant. cAMP_e is the extracellular cAMP concentration in the extracellular volume V_e. $J_{\mathrm{cAMP}i}$ and $J_{\mathrm{cAMP}e}$ (mol sec^{-1} $\mu\mathrm{m}^{-2}$) are the cAMP flows into the extracellular space through the surface S_i ($\mu\mathrm{m}^2$) of an individual cell and through the surface S_m ($\mu\mathrm{m}^2$) of multiple surrounding cells, respectively. PDE_e is the extracellular phosphodiesterase, expressed on the surface of *Dictyostelium*. k_3 is the enzymatic activity of the extracellular phosphodiesterase, k_{PDE} (mol) is the cAMP_e-PDE dissociation constant. ERK2 is the phosphorylated state of the ERK2 protein. n_2 is the phosphorylation rate of ERK2 by PKA, n_1 is the dephosphorylation rate of ERK2 by protein phosphatase Phos. l_1 is the phosphorylation rate by PKA, l_2 is the dephosphorylation rate by the protein phosphatase Phos. ERK 2_0 and ACA_0 are the total concentrations of ERK2 and ACA, respectively.

In order to present the model more conveniently, we have chosen the concentration units to be in $\mu\mathrm{mol}\ \mathrm{l}^{-1} = d$ and time in seconds. Normalization of concentrations by d allows a transformation to new variables:

$$
\mathrm{ca}_i^{2+} = \frac{[\mathrm{Ca}_i^{2+}]}{d}, \mathrm{ca}_{\mathrm{ER}}^{2+} = \frac{[\mathrm{Ca}_{\mathrm{ER}}^{2+}]}{d}, \mathrm{ip3} = \frac{[\mathrm{IP}_3]}{d}, \mathrm{camp}_i = \frac{[\mathrm{cAMP}_i]}{d},
$$

$$
\mathrm{camp}_e = \frac{[\mathrm{cAMP}_e]}{d}, \mathrm{erk2} = \frac{[\mathrm{ERK2}]}{d}, \mathrm{aca} = \frac{[\mathrm{ACA}]}{d}
$$

All Michaelis constants are also dimensionalized by d: $k_m = \frac{K_m}{d}$.

The system (1) in the normalized form is transformed as follows:

$$
\begin{aligned}
\frac{\mathrm{d}(\mathrm{ca}_i^{2+})}{\mathrm{d}t} &= a_1\cdot\left(\psi_i - 0.5\cdot\ln\left(\frac{\mathrm{ca}_{\mathrm{out}}^{2+}}{\mathrm{ca}_i^{2+}}\right)\right) - a_2\cdot p_{\mathrm{PM}}^1(\mathrm{ca}_i^{2+})\\
&\quad + a_3\cdot p_{\mathrm{ER}}^{\mathrm{Ca}^{2+}}\cdot u_{\mathrm{ER}} - a_4\cdot p_{\mathrm{ER}}^1(\mathrm{ca}_i^{2+})\cdot p_{\mathrm{ER}}^2(\mathrm{ca}_{\mathrm{ER}}^{2+}),\\
\frac{\mathrm{d}(\mathrm{ca}_{\mathrm{ER}}^{2+})}{\mathrm{d}t} &= \frac{V_i - V_{\mathrm{ER}}}{V_{\mathrm{ER}}}\cdot(-a_3\cdot p_{\mathrm{ER}}^{\mathrm{Ca}^{2+}}\cdot\mathrm{ca}_{\mathrm{ER}}^{2+} + a_4\cdot p_{\mathrm{ER}}^1(\mathrm{ca}_i^{2+})\\
&\quad\cdot p_{\mathrm{ER}}^2(\mathrm{ca}_{\mathrm{ER}}^{2+})),\\
\frac{\mathrm{d}(\mathrm{ip3})}{\mathrm{d}t} &= m_0\cdot\frac{\mathrm{camp}_e}{k_G + \mathrm{camp}_e} + m_1\cdot\frac{(\mathrm{ca}_i^{2+})^4}{(k_{\mathrm{Ca}^{2+}} + \mathrm{ca}_i^{2+})^4}\\
&\quad + ap - m_2\cdot\frac{\mathrm{ip3}}{k_{ip} + \mathrm{ip3}},\\
\frac{\mathrm{d}(\mathrm{camp}_i)}{\mathrm{d}t} &= D_{\mathrm{ACA}}\cdot\mathrm{aca}^* - j_{\mathrm{cAMP}i} - \mathrm{RegA}_i\cdot\frac{\mathrm{camp}_i}{k_{\mathrm{RegA}} + \mathrm{camp}_i}\\
&\quad\cdot\frac{k_{\mathrm{ER}}}{k_{\mathrm{ER}} + \mathrm{ca}_{\mathrm{ER}}^{2+}},\\
\frac{\mathrm{d}(\mathrm{camp}_e)}{\mathrm{d}t} &= j_{\mathrm{cAMP}i} + j_{\mathrm{cAMP}e} - \mathrm{PDE}_e\cdot\frac{\mathrm{camp}_e}{k_{\mathrm{PDE}} + \mathrm{camp}_e},\\
\frac{\mathrm{d}(\mathrm{erk2})}{\mathrm{d}t} &= d_1\cdot\left(\frac{\mathrm{pka}}{c_1}\cdot(1 - \mathrm{erk2}) - \mathrm{erk2}\right),\\
\frac{\mathrm{d}(\mathrm{aca})}{\mathrm{d}t} &= d_2\cdot\left(\frac{\mathrm{pka}}{c_2}\cdot(1 - \mathrm{aca}) - \mathrm{aca}\right).
\end{aligned}
\tag{2}
$$

where a_1 represents the sum of currents into the membrane, a_2 is the maximum Ca^{2+} current flow through the PMCAs, a_3 is the maximum Ca^{2+} current flow through $\mathrm{IP}_3\mathrm{Rs}$, and a_4 is the max Ca^{2+} current flow through the SERCAs. m_0 and m_1 are the max PLC hydrolysis rates, mediated by the G-protein and Ca^{2+} pathways, respectively, m_2 is the max $\mathrm{IP}_3\mathrm{K}$ hydrolysis rate, ap is the basal level of PIP_2 hydrolysis, reg_i represents normalized activity of RegA, $j_{\mathrm{cAMP}i}$ and $j_{\mathrm{cAMP}e}$ are the normalized flows of cAMP released by an individual *Dictyostelium* cell and surrounding cells, respectively. ψ_i is the cytoplasmic membrane potential, $\psi_i = \frac{F\cdot V_m}{R\cdot T}$, where V_m is the cytoplasmic transmembrane potential. $\mathrm{aca}^* = (1 - \mathrm{aca})\cdot\mathrm{ACA}_{\mathrm{enz}}$ is a normalized function of ACA activity, D_{ACA} is the max ACA hydrolysis rate, RegA_i is the max RegA hydrolysis rate, k_{RegA} is cAMP affinity to RegA, and k_{ER} is modulation of RegA activity by Ca^{2+} release from ER. d_1 and

d_2 are the normalized phosphatase activities that dephosphorylate ERK2 and ACA, respectively. c_1 and c_2 are the complex ratios of the phosphatase and the protein kinase-donor protein complex (ERK2 and ACA, respectively), multiplied by the phosphorylation/dephosphorylation constants as defined in eqn (29).

Derivation of the Ca^{2+} module equations

The first two parts of eqn (2) represent the Ca^{2+} concentration alterations in a given volume due to the flows through membranes and channels. The Nernst–Planck current density equation,[69,70] has been employed in order to make the transition from Ca^{2+} ion flows to Ca^{2+} currents:

$$J = \frac{I}{z \cdot F}, \quad (3)$$

where I is a current generated by a flow J, F is the Faraday's constant, z is the Ca^{2+} ion charge. Eqn (3) allows the representation of the intracellular and ER Ca^{2+} concentration alterations as a sum of Ca^{2+} currents:

$$\frac{\mathrm{d}(\mathrm{ca}_i^{2+})}{\mathrm{d}t} = \sum_i I_i$$
$$\frac{\mathrm{d}(\mathrm{ca}_{ER}^{2+})}{\mathrm{d}t} = \sum_j I_j \quad (4)$$

Below we derive the terms for the currents I through the PMCA, SERCA and IP_3Rs.

The PMCA binds one ion per cycle and extrudes Ca^{2+} to the extracellular space (using the ATP hydrolysis energy), when it is bound to calmodulin with four Ca^{2+} ions. The term for PMCA activation when ca_i^{2+} = const (extracellular Ca^{2+} concentration is approximately 1 mM) is given by the following equations:

$$I_{\mathrm{PM}}^{A}(\mathrm{ca}_i^{2+}, \mathrm{ca}_{\mathrm{out}}^{2+}) = N_{\mathrm{PM}}^{A} \cdot i_{\mathrm{PM}}^{A} \cdot p_{\mathrm{PM}}^{1}(\mathrm{ca}_i^{2+}) \cdot p_{\mathrm{PM}}^{2}(\mathrm{ca}_{\mathrm{out}}^{2+}) = j_{\mathrm{PM}}^{A} \cdot p_{\mathrm{PM}}^{1}(\mathrm{ca}_i^{2+}),$$
$$p_{\mathrm{PM}}^{1}(\mathrm{ca}_i^{2+}) = \frac{\mathrm{ca}_i^{2+}}{k_a^i + \mathrm{ca}_i^{2+}} \cdot \frac{\mathrm{CaM}(\mathrm{ca}_i^{2+})}{k_{\mathrm{CaM}} + \mathrm{CaM}(\mathrm{ca}_i^{2+})}, \ p_{PM}^2 = \frac{k_a^{\mathrm{out}}}{k_a^{\mathrm{out}} + \mathrm{ca}_{\mathrm{out}}^{2+}}, \quad (5)$$

where $j_{\mathrm{PM}}^{A} = N_{\mathrm{PM}}^{A} \cdot i_{\mathrm{PM}}^{A} \cdot \frac{k_a^{\mathrm{out}}}{k_a^{\mathrm{out}} + \mathrm{ca}_{\mathrm{out}}^{2+}}$ is the maximal value of the Ca^{2+} current generated by cytoplasmic Ca^{2+} pumps through one μm^2. k_a^i, k_a^{out} are the equilibrium dissociation constants in the Ca^{2+} and PMCA interactions, on the intracellular and extracellular sides of the cytoplasmic membrane, respectively. N_{PM}^{A} (μm^{-2}) is the number of PMCAs in one μm^2 of cytoplasmic membrane, i_{PM}^{A} is the time-averaged current per single activated PMCA channel. p_{PM}^{1} (ca_i^{2+}) is the probability of one Ca^{2+} ion binding PMCA, and p_{PM}^{2} (ca_i^{2+}) is the probability of Ca^{2+} ions being released by PMCAs on the outer side of the cytoplasmic membrane. Calmodulin activation by Ca^{2+} is modeled as $\mathrm{CaM}(\mathrm{ca}_i^{2+}) = \frac{(\mathrm{ca}_i^{2+})^4}{(k_m + \mathrm{ca}_i^{2+})^4}$, because PMCA requires activated calmodulin to be active itself. k_m is the calmodulin affinity constant for Ca^{2+}, and $P_1 = \frac{K_m^{\mathrm{CaM}}}{[\mathrm{CaM0}]}$ is the calmodulin affinity constant to PMCA divided by total calmodulin concentration.

Various cells have different types of Ca^{2+} channels on the cytoplasmic membrane, the conductivity of which can depend on transmembrane potential, ligands, *etc*. SACs are one such example, since the activation of these channels is driven by membrane tensions, transmembrane potential, and possibly other factors. Currents through Ca^{2+} channels located on cytoplasmic membrane are modelled as:

$$I_{\mathrm{PM}}^{\mathrm{in}} = (N_{\mathrm{PM}}^{\mathrm{Ca}}(S) + N_{\mathrm{PM}}^{\mathrm{Ca}}(G_0)) \cdot i_{\mathrm{PM}}^{\mathrm{in}},$$
$$i_{\mathrm{PM}}^{\mathrm{in}} = -g_{\mathrm{PM}}^{\mathrm{Ca}} \cdot \frac{R \cdot T}{F}\left(\psi_i - 0.5 \cdot \ln\left(\frac{\mathrm{ca}_{\mathrm{out}}^{2+}}{\mathrm{ca}_i^{2+}}\right)\right), \quad (6)$$

where $g_{\mathrm{PM}}^{\mathrm{Ca}}$ is the average conductivity of a single Ca^{2+} channel, $N_{\mathrm{PM}}^{\mathrm{Ca}}(S)$ is the number of SACs in the active (open) state, $N_{\mathrm{PM}}^{\mathrm{Ca}}(G_0)$ is the number of other Ca^{2+} channels in the active state located on the cytoplasmic membrane, and ψ_i is the cytoplasmic transmembrane potential.

SERCA pumps sequester Ca^{2+} to the ER and each bind two Ca^{2+} ions per ATP hydrolysis cycle. The term for SERCA pumps is described by the equation:

$$I_{\mathrm{ER}}^{A}(\mathrm{ca}_i{}^{2+}, \mathrm{ca}_{\mathrm{ER}}{}^{2+}) = N_{\mathrm{ER}}^{A} \cdot i_{\mathrm{ER}}^{A} \cdot p_{\mathrm{ER}}^{1}(\mathrm{ca}_i{}^{2+}) \cdot p_{\mathrm{ER}}^{2}(\mathrm{ca}_{\mathrm{ER}}{}^{2+}), \quad (7)$$

where N_{ER}^{A} is the number of SERCAs per one μm^2 of the ER membrane, i_{ER}^{A} is the time-averaged current through a single channel, $p_{\mathrm{ER}}^{1}(\mathrm{ca}_i{}^{2+})$ is the probability of two Ca^{2+} ions binding to ATPase, and $p_{\mathrm{ER}}^{2}(\mathrm{ca}_i{}^{2+})$ is the probability of Ca^{2+} ion release by SERCAs. If the two Ca^{2+} ions have a consecutive binding mechanism, then Ca^{2+} binding and release probabilities are given as:

$$p_{\mathrm{ER}}^{1}(\mathrm{ca}_i^{2+}) = \frac{(\mathrm{ca}_i^{2+})^2}{k^2 + k \cdot \mathrm{ca}_i^{2+} + (\mathrm{ca}_i^{2+})^2},$$
$$p_{\mathrm{ER}}^{2}(\mathrm{ca}_{ER}^{2+}) = \frac{k_1^2}{k_1^2 + k_1 \cdot \mathrm{ca}_{\mathrm{ER}}^{2+} + (\mathrm{ca}_{\mathrm{ER}}^{2+})^2}. \quad (8)$$

In the case of the ER, Ca^{2+} concentration can vary over a wide range on both sides of the ER membrane; this situation is essentially different from the description of Ca^{2+} currents through the cytoplasmic membrane, because the extracellular concentration does not vary nearly as much. Thus, in the ER case, equations similar to eqn (6) can no longer be used. The passive currents through the ER membrane, therefore, were presented differently from currents through the cytoplasmic membrane. General equations.[71] for currents that depend on both internal and external ion concentrations are:

$$\begin{aligned} I_{\mathrm{ER}}^{\mathrm{in}} &= N_{\mathrm{ER}}^{\mathrm{Ca}} \cdot p_{\mathrm{ER}}^{\mathrm{Ca}} \cdot i_{\mathrm{ER}}^{\mathrm{Ca}} , i_{\mathrm{ER}}^{\mathrm{in}} \\ &= z \cdot F \cdot \nu \cdot ([\mathrm{Ca_{ER}}{}^{2+}] \cdot \exp(n \cdot z \cdot (\psi_0 - \psi_{\mathrm{ER}})) \\ &\quad - [\mathrm{Ca}_i{}^{2+}] \cdot \exp(-n \cdot z \cdot (\psi_0 - \psi_{\mathrm{ER}}))), \end{aligned} \quad (9)$$

where $N_{\mathrm{ER}}^{\mathrm{Ca}_{\mathrm{ER}}^{2+}}$ is the total number of passive Ca^{2+} channels per μm^2 on the ER membrane, p_{ER}^{1} is the probability for a single IP_3R of being open, $i_{\mathrm{ER}}^{\mathrm{in}}$ is the time-averaged current through activated single IP_3R, n is a parameter representing the structure of electrostatic potential distribution throughout the channel, $\psi_0 = \frac{F \cdot \varphi_0}{R \cdot T}$ and $\psi_{ER} = \frac{F \cdot \varphi_{\mathrm{ER}}}{R \cdot T}$, φ_0 is an equilibrium potential of the cytoplasmic membrane, and φ_{ER} is the membrane potential of the ER.

Downloaded by University of Northumbria on 15 October 2012
Published on 16 April 2009 on http://pubs.rsc.org | doi:10.1039/B822074C

 This journal is © The Royal Society of Chemistry 2009

Published on 16 April 2009 on http://pubs.rsc.org | doi:10.1039/B822074C
Downloaded by University of Northumbria on 15 October 2012

Given that $u_{ER} \sim 10^{-4}$ M >> 10^{-6} M $\approx u_i$ and $e^k >> e^{-k}$ (for $k >> 0$) we can approximate the current through single IP_3Rs as:

$$i_{ER}^{in} \approx z \cdot F \cdot \nu \cdot \exp(n \cdot z \cdot (\psi_0 - \psi_{ER})) \cdot [Ca_{ER}^{2+}],$$

Structural[72] and physiological[38] studies lead to the following equation for Ca^{2+}- and IP_3-dependent probability of IP_3Rs being open:

$$p_{ER}^{Ca^{2+}} = p_{st} + j_{ER}^{in} \cdot \frac{k_{ca}^4 \cdot (ca_i^{2+})^8 \cdot (1 - p_{st})}{(ca_i^{2+})^8 + (k_{ca} + ca_i^{2+})^{12} \cdot Kk} \cdot \frac{ip3^4}{(k_{ins} + ip3)^4} + j_{IP_3} \frac{ip3^4}{(k_{ins} + ip3)^4}, \quad (10)$$

where p_{st} is the Ca^{2+}- and IP_3-independent basal level of probability for the channel to be open, $Kk = \frac{k_{close}}{k_{open}}$ and k_{close} is the IP_3 channel closing rate, k_{open} is the IP_3 channel opening rate and k_{ca} is the equilibrium dissociation constant in the reaction where Ca^{2+} interacts with the IP_3R channel. k_{ins} is the IP_3 binding affinity constant. This equation explicitly incorporates all four IP_3 and twelve Ca^{2+} binding sites in determining the conductance of the IP_3R channel.

Derivation of the IP_3 module equation

The protein activities that regulate the IP_3 concentration (third line in eqn (2)) are given according the following considerations. Fig. 1 schematically illustrates the IP_3 formation and degradation pathways. PIP_2 hydrolysis by PLC is the source of IP_3, and further phosphorylation by IP_3K decreases the concentration of IP_3 in the cytoplasm. PLC in *Dictyostelium* is reported to be regulated by both Ca^{2+} and G-protein subunits.[44] PLC has four Ca^{2+} binding sites formed by EF hands. PLC activity in our model is represented by Ca^{2+}-dependent and Ca^{2+}-independent terms reflecting the Ca^{2+}-dependence and extracellular factor-dependence *via* the G-protein pathway:

$$\begin{aligned} &\mathrm{PLC}(u_i, \text{ extracellular cAMP}) \\ &= \mathrm{PLC}_{Ca^{2+}} + \mathrm{PLC}_G \\ &= N_{\mathrm{PLC}_{Ca^{2+}}} \cdot \frac{(ca_i^{2+})^4}{(k_{Ca^{2+}} + ca_i^{2+})^4} + N_{\mathrm{PLC}_G} \cdot \frac{camp_e}{k_G + camp_e}, \end{aligned} \quad (11)$$

where k_{ca2+} is the Ca^{2+} affinity constant for PLC, $k_{PLC^{2+}_{Ca}}$ and k_{PLC_G} are the coefficients that define the contributions to the PLC activation by the Ca^{2+} and G-protein pathways, respectively, $camp_e$ is the extracellular cAMP concentration, k_G is the equilibrium dissociation constant for the extracellular cAMP binding to cAR1.

In our model, IP_3 is further phosphorylated into IP_4 by IP_3K. Although IP_3 can also be dephosphorylated into IP_2, we find that incorporation of the IP_3 dephosphorylation term into the model does not lead to any significant effects, and we have, therefore, only considered the phosphorylation reaction of IP_3 into IP_4. The stationary velocity of this reaction is given by:

$$IP_3K(ip3) = \mu_{IP_3K} \cdot \frac{ip3}{k_{ip} + ip3}, \quad (12)$$

where k_{ip} is the Michaelis constant and μ_{IP_3K} is the maximal rate of IP_3 conversion into IP_4.

Derivation of the G protein-coupled module equations

The module that includes the intra- and extracellular cAMP alterations (fourth and fifth lines in eqn (2)) is represented mathematically as follows. Extracellular cAMP binds to cAR1 which in turn regulates the activities of ERK2 and ACA *via* G-proteins.[73,74] Since the activation of ERK2 appears to depend on cAR1 activation, so that both oscillate in the same phase,[22,23] cAR1 was not included into the model as an independent variable. On the other hand, ACA has been reported to depend on intracellular Ca^{2+}.[36,75] As mentioned earlier, given the lack of detailed biochemical characterization of ACA dependence on Ca^{2+}, various ACA activation mechanisms were tested computationally in the model, *via* the CaM protein, in analogy with the mammalian adenylyl cyclases. Since the interplay of signals *via* the cAR1/G-protein pathways and Ca^{2+} signals can have a highly non-linear nature, a comprehensive dependence of ACA on these two factors has been developed in our model.

ACA in this model is assumed to be indirectly activated by Ca^{2+}-CaM pairs and by two-types of G-proteins: G2 $\beta\gamma$ subunits *via* CRAC protein[36,76] and Gα3 subunits.[77] The cAMP production rate by an individual ACA_i complex is given by:

$$\mu_i = \frac{k_{ACA}^i \cdot ACA_i \cdot ATP}{K_{ATP} + ATP} \quad (13)$$

where K_{ATP} is the equilibrium dissociation constant for the ACA-ATP interaction, and $\sum_i ACA_i = ACA_0$, where ACA_0 is the total concentration of ACA.

The total cAMP production rate is given by the sum of the individual production rates of ACA-CaM or ACA-G-protein subunit complexes as defined by eqn (13). Thus,

$$\mu_{cAMP} = \sum_i \mu_i \quad (14)$$

Where the probability of ACA to be activated by Ca^{2+}-CaM and with G-proteins is given by the following probabilities:

$$ACA_{enz} = ACA_0 \cdot p_{CaM}^{C1_i} \cdot p_{G_1}^{C2_i} \cdot p_{G_2}^{C3_i}, \quad (15)$$

where $p_{CaM}^{C1_i}$, $p_{G_1}^{C2_i}$, and $p_{G_2}^{C3_i}$ are the probabilities for ACA regulation by CaM bound to a number of Ca^{2+} ions, and with the two types of G-protein pathways, respectively.

The probabilities for CaM-ACA interactions are given by:

$$p_{CaM}^{C1=1} = \frac{CaM}{K_{CaM-ACA} + CaM}, \quad p_{CaM}^{C1=0} = \frac{K_{CaM-ACA}}{K_{CaM-ACA} + CaM}. \quad (16)$$

where p_{CaM}^1 and p_{CaM}^0 are the probabilities of ACA to be in a complex with and without CaM, respectively. $C1_i = 1$ if

View Online

Downloaded by University of Northumbria on 15 October 2012
Published on 16 April 2009 on http://pubs.rsc.org | doi:10.1039/B822074C

$i = 1,\ldots,4$, $C1_i = 0$, when $i = 5,\ldots,8$, and $K_{\text{caM-ACA}}$ is the equilibrium dissociation constant for CaM-ACA interactions.

The probabilities for G_1-ACA interactions are given by:

$$p_{G_1}^{C2=1} = \frac{G_1}{K_{G_1} + G_1}, \quad p_{G_1}^{C2=0} = \frac{K_{G_1}}{K_{G_1} + G_1}. \tag{17}$$

where $p_{G_1}^1$ and $p_{G_1}^0$ are the probabilities of ACA to be in a complex with and without G_1, respectively. C2 = 1 when i = 2,4,6,8, C2 = 0 if i = 1,3,5,8. $K_{G_1\text{-ACA}}$ is the equilibrium dissociation constant for G_1-ACA interactions. Similarly, for the second type of G-protein subunit we have:

$$p_{G_2}^{C3=1} = \frac{G_2}{K_{G_2} + G_2}, \quad p_{G_2}^{C3=0} = \frac{K_{G_2}}{K_{G_2} + G_2}. \tag{18}$$

where $p_{G_2}^1$ and $p_{G_2}^0$ are the probabilities of ACA to be in a complex with and without G_2, respectively. C3 = 1 if i = 2,4,6,8, C3 = 0 when i = 1,3,5,8, $K_{G_2\text{-ACA}}$ is the equilibrium dissociation constant for G_2-ACA interactions.

ACA is activated by CaM with j = 0, 1, or 2 bound Ca^{2+} ions. Fig. 3 shows the normalized ACA dependence on Ca^{2+} and G-protein concentrations for these 3 cases. A more detailed description of Ca^{2+}-CaM-dependent regulation can be found in ref. 47, 48 and 78.

Additional complexity in the dynamics of ACA activity modulation comes from the PKA phosphorylation of the cAR1 receptor. Since cAR1 activation by extracellular cAMP has been shown to activate ACA almost linearly, the cAR1 receptor has not been included as an independent state variable in the model. However, the effects of cAR1 phosphorylation by cAMP-dependent PKA and the associated effects on the level of ACA have been modelled according to eqn (26), as discussed in the section on phosphorylation dynamics below.

Intracellular cAMP is produced by ACA and hydrolysed by intracellular phosphodiesterase RegA. The activity of RegA is given by:

$$\text{RegA}(\text{Ca}_i^{2+}, \text{ERK2}) = \text{RegA}_0 \cdot \left(\frac{k_{\text{ERK2}}}{k_{\text{ERK2}} + \text{erk2}} + \text{regA}_{st}\right). \tag{19}$$

where RegA_0 is the total RegA concentration, k_{ERK2} is the equilibrium dissociation constant for RegA interaction with ERK2, regA_{st} is the stationary RegA activity in the absence of any stimulation.

The release of cAMP from the intracellular space into the extracellular compartment is modelled as the sum of intracellular cAMP and Ca^{2+} terms:

$$J_{\text{cAMP}i} = \frac{V_e \cdot d}{S_i} \cdot \left(K_{\text{out}}^{\text{cAMP}} \cdot \frac{(\text{camp}_i)^2}{(k_{\text{cAMP}} + \text{camp}_i)^2} - K_{\text{out}}^{\text{Ca}^{2+}} \cdot \frac{\text{ca}_i^{2+}}{k_{\text{Ca}^{2+}} + \text{ca}_i^{2+}}\right). \tag{20}$$

where $K_{\text{out}}^{\text{cAMP}}$ and $K_{\text{out}}^{\text{Ca}^{2+}}$ are the relative strengths of the cAMP and Ca^{2+}-dependent terms of the cAMP release, and k_{cAMP} and $k_{\text{Ca}^{2+}}$ describe the sensitivity of cAMP release to intracellular cAMP and Ca^{2+} concentrations, respectively. The activation of PKA by intracellular cAMP is given by:

$$\text{PKA} = \text{PKA}_0 \cdot \left(\frac{\text{camp}}{k_{\text{PKA}} + \text{camp}}\right)^4. \tag{21}$$

where PKA_0 is the total PKA concentration, and k_{PKA} is the equilibrium dissociation constant for cAMP-PKA interactions.

Relationship between parameters in original and normalised model equations

The relationship between the parameters in the normalized system of differential equations with the original description for the flows in the cellular volume is thus given by:

$$\begin{aligned}
a_1 &= \frac{S_i \cdot N_{\text{PM}}^{\text{Ca}} \cdot g_{\text{PM}}^{\text{Ca}} \cdot R \cdot T}{z \cdot F^2 \cdot (V_i - V_{\text{ER}}) \cdot d} = \frac{j_{\text{PM}}^{\text{in}}}{d}, \\
a_2 &= \frac{S_i \cdot \tau_1}{z \cdot F \cdot (V_i - V_{\text{ER}}) \cdot d} = \frac{j_{\text{PM}}^{A}}{d}, \\
a_3 &= \frac{S_{\text{ER}} \cdot N_{\text{ER}}^{i} \cdot \nu \cdot \exp(n \cdot z \cdot (\psi_0 - \psi_{\text{ER}}))}{(V_i - V_{\text{ER}})} = \frac{j_{\text{ER}}^{\text{in}}}{d}, \\
a_4 &= \frac{S_{\text{ER}} \cdot N_{\text{ER}}^{A} \cdot i_{\text{ER}}^{A}}{z \cdot F \cdot (V_i - V_{\text{ER}}) \cdot d} = \frac{j_{\text{ER}}^{A}}{d}, \\
m_0 &= \frac{r_0 \cdot S_i^2 \cdot N_{\text{PLC}_{\text{Ca}^{2+}}} \cdot [\text{PIP}_2]}{(V_i - V_{ER}) \cdot d} = \frac{\mu_{\text{PLC}_{\text{Ca}^{2+}}}}{d}, \\
m_1 &= \frac{r_1 \cdot S_i^2 \cdot N_{\text{PLC}_G} \cdot [\text{PIP}_2]}{(V_i - V_{ER}) \cdot d} = \frac{\mu_{\text{PLC}_G}}{d}, \\
m_2 &= \frac{\mu_{\text{IP3}K}}{d}, \\
ap &= \frac{r \cdot S_i^2 \cdot N_{\text{PLC}} \cdot [\text{PIP}_2]}{N^A \cdot (V_i - V_{\text{ER}}) \cdot d} = \frac{\mu_{\text{PLCst}}}{d}, \\
\frac{V_i - V_{\text{ER}}}{V_{\text{ER}}} &\approx 4.4.
\end{aligned} \tag{22}$$

The final system of differential equations, which were solved numerically to generate all the results presented in the paper is thus given by:

$$\begin{aligned}
\frac{\text{d}(\text{ca}_i^{2+})}{\text{d}t} = {} & j_{\text{PM}}^{\text{in}} \cdot \left(\psi_i - 0.5 \cdot \ln\left(\frac{\text{ca}_{\text{out}}^{2+}}{\text{ca}_i^{2+}}\right)\right) \\
& - j_{\text{PM}}^{A} \cdot \frac{\text{ca}_i^{2+}}{k_a^i + \text{ca}_i^{2+}} \cdot \frac{\text{CaM}(\text{ca}_i^{2+})}{k_{\text{CaM}} + \text{CaM}(\text{ca}_i^{2+})} \\
& + j_{\text{ER}}^{\text{in}} \cdot p_{\text{ER}}^{\text{Ca}^{2+}} \cdot \text{ca}_{\text{ER}}^{2+} - a_4 \cdot p_{\text{ER}}^{1} \cdot p_{\text{ER}}^{2},
\end{aligned}$$

 This journal is © The Royal Society of Chemistry 2009

View Online

$$\frac{d(ca_{ER}^{2+})}{dt} = \frac{V_i - V_{ER}}{V_{ER}} \cdot (-j_{ER}^{in} \cdot p_{ER}^{Ca^{2+}} \cdot ca_{ER}^{2+} + a_4 \cdot p_{ER}^{1} \cdot p_{ER}^{2}),$$

$$\frac{d(ip3)}{dt} = \mu_{PLC_{Ca^{2+}}} \cdot \frac{(ca_i^{2+})^4}{(k_{Ca^{2+}} + ca_i^{2+})^4} + \mu_{PLC_G} \cdot \frac{camp_e}{k_G + camp_e} + ap - \mu_{IP_3K} \cdot \frac{ip3}{k_{ip} + ip3}, \quad (23)$$

$$\frac{d(camp_i)}{dt} = D_{ACA} \cdot aca^* - RegA_i \cdot \frac{camp_i}{k_{RegA} + camp_i} \cdot \frac{k_{ER}}{k_{ER} + ca_{ER}^{2+}} - K_{out}^{cAMP} \cdot \frac{(camp_i)^2}{(k_{cAMP} + camp_i)^2} - K_{out}^{Ca^{2+}} \cdot \frac{ca_i^{2+}}{k_{Ca^{2+}} + ca_i^{2+}},$$

$$\frac{d(camp_e)}{dt} = K_{out}^{cAMP} \cdot \frac{(camp_i)^2}{(k_{cAMP} + camp_i)^2} \cdot (camp_i - camp_e) + K_{out}^{Ca^{2+}} \cdot \frac{ca_i^{2+}}{k_{Ca^{2+}} + ca_i^{2+}} - PDE_e \cdot \frac{camp_e}{k_{PDE} + camp_e},$$

$$\frac{d(erk)}{dt} = d_1 \cdot \left(\frac{pka}{c_1} \cdot (1 - erk) - erk\right)$$

$$\frac{d(aca)}{dt} = d_2 \cdot \left(\frac{pka}{c_2} \cdot (1 - aca) - aca\right)$$

where j_{PM}^{in} represents the sum of currents into the membrane, j_{PM}^{A} is the max Ca^{2+} current flow through the PMCAs, j_{ER}^{in} is the max Ca^{2+} current flow through the IP_3Rs, j_{ER}^{A} is the max

Table 2 Model parameters

Symbol	Value	Meaning
j_{PM}^{in}	0.05 μM sec^{-1}	The sum of currents into the membrane
j_{PM}^{A}	12 μM sec^{-1}	Max Ca^{2+} flow through PMCAs
j_{ER}^{in}	0.1 μM sec^{-1}	Max current flow through IP_3Rs
j_{IP3}	0.3 μM sec^{-1}	Max current flow through IP_3 "proportion" of IP_3Rs
j_{ER}^{A}	20000 μM sec^{-1}	Max Ca^{2+} flow through SERCA
k_a^i	0.4 μM	PMCA Ca^{2+} affinity
V_{ER}/V_i	0.185	ER to cell volumes ratio
Kk	0.00025	Ratio of IP_3R opening to closing rates
k_{ins}	0.1 μM	IP_3 binding affinity to IP_3R
k_{ca}	0.12 μM	Ca^{2+} binding affinity to IP_3R
k_m	1 μM	Ca^{2+} affinity to CaM
k_{CaM}	0.003 μM	CaM affinity to PMCA
k_δ	0.4 μM	Ca^{2+} binding affinity to PLC
k_β	0.4 μM	Sensitivity of PLC to extracellular cAMP-cAR1 interactions
$\mu_{PLC_{Ca}^{2+}}$	0.7 μM s^{-1}	Max Ca^{2+}-dependent PLC hydrolysis rate
μ_{PLC_G}	0.1 μM s^{-1}	Max G-protein pathway PLC hydrolysis rate
μ_{PLCst}	0.01 μM s^{-1}	Basal level of PLC hydrolysis rates
k_{ip}	1 μM	IP_3 binding affinity to IP_3K
μ_{IP4K}	0.5 μM sec^{-1}	Max IP_3K hydrolysis rate
k_{PKA}	0.1 μM	Equilibrium dissociation constant for cAMP-PKA interactions
φ_i	−70 mV	Resting membrane potential of cytoplasm
φ_{ER}	−70 mV	Resting membrane potential of ER
D_{ACA}	3.6 μM s^{-1}	Max ACA hydrolysis rate
$RegA_i$	138 μM s^{-1}	Max RegA hydrolysis rate
K_{out}^{cAMP}	4000 μM sec^{-1}	Relative strength of the cAMP-dependent cAMP release
$K_{out}^{Ca^{2+}}$	3000 μM sec^{-1}	Relative strength of the Ca^{2+}-dependent cAMP release
k_{cAMP}	0.5 μM	Sensitivity of cAMP release to intracellular cAMP concentration
$k_{Ca^{2+}}$	0.3 μM	Sensitivity of cAMP release to intracellular Ca^{2+} concentration
k_{RegA}	0.1 μM	cAMP affinity to RegA
k_{ER}	0.1 μM	Modulation of RegA activity by Ca^{2+} release from ER
PDE_e	1580 μM sec^{-1}	Max extracellular PDE hydrolysis rate
k_{PDE}	0.2 μM	cAMP affinity to extracellular PDE
c_1	0.75	Defined by eqn (29)
c_2	0.625	Defined by eqn (29)
d_1	0.5 μM sec^{-1}	ERK2 dephosphorylation rate
d_2	0.5 μM sec^{-1}	ERK2 dephosphorylation rate
k_{ACA}^i	0, 300, 100, 100, 100, 100 μM sec^{-1}	ACA activities in complex with variable combinations of CaM and/or G-protein subunits bound
k_{ATP}	1 μM	Equilibrium dissociation constant for ACA-ATP interaction
ATP	4×10^3 μM	ATP concentration
$K_{caM\text{-}ACA}$	0.1 μM	Equilibrium dissociation constant for CaM-ACA interaction
$K_{G\text{-}ACA}$	0.5 μM	Equilibrium dissociation constant for G-ACA interaction

Downloaded by University of Northumbria on 15 October 2012
Published on 16 April 2009 on http://pubs.rsc.org | doi:10.1039/B822074C

Downloaded by University of Northumbria on 15 October 2012
Published on 16 April 2009 on http://pubs.rsc.org | doi:10.1039/B822074C

current flow through the SERCAs, $\mu_{\mathrm{PLC}^{2+}_{\mathrm{Ca}}}$ and μ_{PLC_G} are the max PLC hydrolysis rates induced by the Ca^{2+} and G-protein pathways, respectively, $\mu_{\mathrm{IP_3K}}$ is the max IP$_3$K hydrolysis rate, μ_{PLCst} is a basal level of PIP$_2$ hydrolysis, aca* = (1 − aca)·ACA$_{\mathrm{enz}}$ is a normalized function of ACA activity, D_{ACA} is the max ACA hydrolysis rate, RegA$_i$ is the max RegA hydrolysis rate, and $K^{\mathrm{cAMP}}_{\mathrm{out}}$ and $K^{\mathrm{Ca^{2+}}}_{\mathrm{out}}$ are the relative strengths of the cAMP- and Ca^{2+}-dependent cAMP release, respectively. k_{RegA} is cAMP affinity to RegA, k_{ER} is the modulation of RegA activity by Ca^{2+} release from ER, and k_{cAMP} and $k_{\mathrm{Ca^{2+}}}$ are the sensitivities of cAMP release to intracellular cAMP and Ca^{2+} concentrations, respectively. d_1 and d_2 are the normalized phosphatase activities that dephosphorylate ERK2 and ACA, respectively. c_1 and c_2 are the complex ratios of the phosphatase and the protein kinase–donor protein complexes (ERK2 and ACA, respectively), multiplied by the phosphorylation/dephosphorylation constants as defined in eqn (29) below.

All parameter values used in the above equations are given in Table 2.

Derivation of a general equation for protein regulation *via* phosphorylation

Since both ACA and ERK2 proteins are regulated by phosphorylation, below we derive a general equation for a protein activity regulated by phosphorylation. Phosphorylation is the addition of a phosphate group to a protein. As a result, the protein may alter its conformation, binding properties to other proteins and ultimately its inherent activity. The removal of the phosphate group is mediated by protein phosphatases. The protein kinase P transfers the phosphate group A from a donor protein D to the protein M, whereas the protein phosphotase F removes the phosphate group A from the protein M. The kinetic scheme for the phosphate addition and removal is shown below:

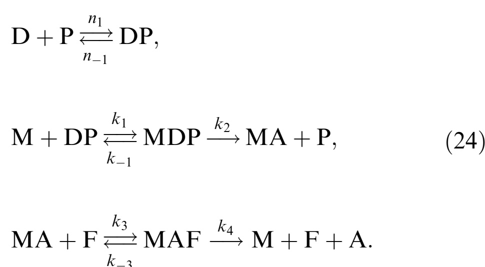

$$\mathrm{D} + \mathrm{P} \underset{n_{-1}}{\overset{n_1}{\rightleftharpoons}} \mathrm{DP},$$
$$\mathrm{M} + \mathrm{DP} \underset{k_{-1}}{\overset{k_1}{\rightleftharpoons}} \mathrm{MDP} \xrightarrow{k_2} \mathrm{MA} + \mathrm{P}, \qquad (24)$$
$$\mathrm{MA} + \mathrm{F} \underset{k_{-3}}{\overset{k_3}{\rightleftharpoons}} \mathrm{MAF} \xrightarrow{k_4} \mathrm{M} + \mathrm{F} + \mathrm{A}.$$

where DP is the donor protein D and the protein kinase P complex, MDP is the DP complex bound to the protein M in the unphosphorylated state, MA is the phosphorylated state of the protein M, MAF is the phosphorylated protein M in a complex with protein phosphatase F. n_1, k_1, and k_3 are the complex assembly rates for the corresponding reactions, while n_{-1}, k_{-1}, k_{-3}, k_2, and k_4 are the complex dissociation rates.

For a biologically realistic case when $[D] >> \frac{n_{-1}}{n_1}$, it is reasonable to assume that most protein kinase P molecules will be in a complex with a donor protein D. In this case the system of differential equations for eqn (24) is given by:

$$\frac{\mathrm{d}M}{\mathrm{d}t} = -k_1 \cdot M \cdot \mathrm{DP} + k_{-1} \cdot \mathrm{MDP} + k_4 \cdot \mathrm{MAF},$$
$$\frac{\mathrm{d\,MA}}{\mathrm{d}t} = -k_3 \cdot \mathrm{MA} \cdot F + k_{-3} \cdot \mathrm{MAF} + k_2 \cdot \mathrm{MDP},$$
$$\frac{\mathrm{d\,MDP}}{\mathrm{d}t} = k_1 \cdot M \cdot \mathrm{DP} - (k_{-1} + k_2) \cdot \mathrm{MDP}, \qquad (25)$$
$$\frac{\mathrm{d\,MAF}}{\mathrm{d}t} = k_3 \cdot \mathrm{MA} \cdot F - (k_{-3} + k_4) \cdot \mathrm{MAF}.$$

We will next consider the pseudo steady-state approximation when the concentrations of the MDP and MAF are constant. In this case, the two last lines of eqn (25) give:

$$\mathrm{MDP} = \frac{k_1}{k_{-1} + k_2} \cdot M \cdot \mathrm{DP},$$
$$\mathrm{MAF} = \frac{k_3}{k_{-3} + k_4} \cdot \mathrm{MA} \cdot F. \qquad (26)$$

By substituting eqn (26) into the second equation from eqn (25), one can obtain:

$$\frac{\mathrm{d\,MA}}{\mathrm{d}t} = -\frac{k_3 \cdot k_4}{k_{-3} + k_4} \cdot \mathrm{MA} \cdot F + \frac{k_1 \cdot k_2}{k_{-1} + k_2} \cdot M \cdot \mathrm{DP}. \qquad (27)$$

Since the sum of the phosphorylated M and unphosphorylated MA molecules is a constant number M_0: M + MA = M_0, eqn (24) can be represented as:

$$\frac{\mathrm{d\,MA}}{\mathrm{d}t} = -\frac{k_3 \cdot k_4}{k_{-3} + k_4} \cdot \mathrm{MA} \cdot F + \frac{k_1 \cdot k_2}{k_{-1} + k_2} \cdot (M_0 - \mathrm{MA}) \cdot \mathrm{DP}. \qquad (28)$$

or in the non-dimensional representation as:

$$\frac{\mathrm{d\,ma}}{\mathrm{d}\tau} = d \cdot \left(\frac{x}{c} \cdot (1 - \mathrm{ma}) - \mathrm{ma}\right). \qquad (29)$$

where $ma = \frac{MA}{M_0}$, $\tau = \frac{k_3 \cdot k_4}{k_{-3}+k_4} \cdot F_0 \cdot t$, $d = \frac{F}{F_0}$, $p = \frac{\mathrm{DP}}{\mathrm{DP_0}}$, $c = \frac{k_3 \cdot k_4 \cdot (k_{-1}+k_2) \cdot F_0}{k_1 \cdot k_2 \cdot (k_{-3}+k_4) \cdot DP_0}$, $x = \frac{p}{d}$, F_0 and DP_0 are the total concentrations of the protein phosphatase and the protein kinase–donor protein complex, respectively.

Eqn (28) and (29) have been used in our model to describe the modulation of the ACA and ERK2 activities when phosphorylated by PKA.[22]

Procedure for comparing the robustness of the proposed model with the G protein-coupled receptor model

The G protein-coupled receptor model analysed in this study is taken from,[22] and may be viewed as a "minimal" model for

 This journal is © The Royal Society of Chemistry 2009

View Online

Downloaded by University of Northumbria on 15 October 2012
Published on 16 April 2009 on http://pubs.rsc.org | doi:10.1039/B822074C

generating stable cAMP oscillations. The set of nonlinear differential equations describing the dynamics of this model are given by:

$$\frac{d[ACA]}{dt} = k_1[CAR1] - k_2[ACA][PKA]$$

$$\frac{d[PKA]}{dt} = k_3[cAMPi] - k_4[PKA]$$

$$\frac{d[ERK2]}{dt} = k_5[CAR1] - k_6[PKA][ERK2]$$

$$\frac{d[RegA]}{dt} = k_7 - k_8[ERK2][RegA]$$

$$\frac{d[cAMPi]}{dt} = k_9[ACA] - k_{10}[RegA][cAMPi]$$

$$\frac{d[cAMPe]}{dt} = k_{11}[ACA] - k_{12}[cAMPe]$$

$$\frac{d[CAR1]}{dt} = k_{13}[cAMPe] - k_{14}[CAR1]$$

where ACA is adenylyl cyclase, PKA is the protein kinase, ERK2 is the mitogen-activated protein kinase, cAMPi and cAMPe are the internal and the external cAMP concentrations, respectively, RegA is the internal cAMP phosphodiesterase and cAR1 is the ligand-bound G protein-coupled receptor. Initial concentrations and nominal values for the parameters in the above model are as given in ref. 22.

To ensure a consistent procedure for checking the robustness of both models, the Monte-Carlo simulation technique is used to simultaneously vary four parameters which determine the dynamics of the extracellular cAMP positive feedback loop in both the minimal and the proposed model. The four parameters which are varied in the minimal model are k_9, k_{10}, k_{11} and k_{12}, while in the proposed model they are D_{ACA}, $RegA_i$, K_{out}^{cAMP} and PDE_e.

For each model, the uncertain parameters are sampled uniformly from the following:

$$\text{param} = \overline{\text{param}}_i(1 + p_\delta \delta_i)$$

where $\overline{\text{param}}_i$ is the nominal value of the parameter i, p_δ is the maximum level of perturbation, *i.e.*, 0.2, 0.4, or 0.6, and δ_i is a uniformly distributed random number between -1 and $+1$.

Although some of the nominal parameter values in each model were derived from (inherently noisy) biological data, others were tuned to values that generated the required oscillatory behaviour. Thus, we have very little *a priori* information on the likely distributions of the parameters as a result of environmental variations and modelling uncertainty. In such cases, the uniform distribution is the standard choice for the type of statistical robustness analysis performed in this paper.[22] The simulations for both models were performed using standard numerical routines in MATLAB.

Acknowledgements

This work was carried out under EPSRC platform grant (EP/D029937/1), BBSRC grant (BB/D015340/1) and by RFBR grant.

References

1 S. Fache, J. Dalous, M. Engelund, C. Hansen, F. Chamaraux, B. Fourcade, M. Satre, P. Devreotes and F. Bruckert, *J. Cell Sci.*, 2005, **118**(15), 3445–3457.
2 M. Clotworthy and D. Traynor, *BMC Cell Biol.*, 2006, **7**, 5.
3 C. L. Saxe, *Am. J. Hum. Genet.*, 1999, **65**, 25–30.
4 R. S. Williams, K. Boeckeler, R. Graf, A. Muller-Taubenberger, Z. Li, R. R. Isberg, D. Wessels, D. R. Soll, H. Alexander and S. Alexander, *Trends Mol. Med.*, 2006, **12**, 415–424.
5 S. S. Willard and P. N. Devreotes, *Eur. J. Cell Biol.*, 2006, **85**, 897–904.
6 I. F. Charo and M. B. Taubman, *Circ. Res.*, 2004, **95**, 858–866.
7 S. A. Eccles, *Curr. Opin. Genet. Dev.*, 2005, **15**, 77–86.
8 L. Trusolino and P. M. Comoglio, *Nat. Rev. Cancer*, 2002, **2**, 289–300.
9 H. L. Ennis and M. Sussman, *Proc. Natl. Acad. Sci. U. S. A.*, 1958, **44**, 401–411.
10 A. Goldbeter, *Bull. Math. Biol.*, 2006, **68**, 1095–1109.
11 M. H. Cohen and A. Robertson, *J. Theor. Biol.*, 1971, **31**, 119–130.
12 M. H. Cohen and A. Robertson, *J. Theor. Biol.*, 1971, **31**, 101–118.
13 H. Parnas and L. A. Segel, *J. Theor. Biol.*, 1978, **71**, 185–207.
14 H. Parnas and L. A. Segel, *J. Cell Sci.*, 1977, **25**, 191–204.
15 S. A. MacKay, *J. Cell Sci.*, 1978, **33**, 1–16.
16 A. Goldbeter and L. A. Segel, *Differentiation*, 1980, **17**, 127–135.
17 A. Goldbeter and L. A. Segel, *Proc. Natl. Acad. Sci. U. S. A.*, 1977, **74**, 1543–1547.
18 P. E. Rapp and M. J. Berridge, *J. Theor. Biol.*, 1977, **66**, 497–525.
19 J. L. Martiel and A. Goldbeter, *Nature*, 1985, **313**, 590–592.
20 P. S. Hagan and M. S. Cohen, *J. Theor. Biol.*, 1981, **93**, 881–908.
21 J. J. Tyson and J. D. Murray, *Development*, 1989, **106**, 421–426.
22 M. Maeda, S. Lu, G. Shaulsky, Y. Miyazaki, H. Kuwayama, Y. Tanaka, A. Kuspa and W. F. Loomis, *Science*, 2004, **304**, 875–878.
23 M. T. Laub and W. F. Loomis, *Mol. Biol. Cell*, 1998, **9**, 3521–3532.
24 D. F. Lusche, K. Bezares-Roder, K. Happle and C. Schlatterer, *BMC Cell Biol.*, 2005, **6**, 12.
25 C. Schlatterer, K. Happle, D. F. Lusche and J. Sonnemann, *J. Biol. Chem.*, 2004, **279**, 18407–18414.
26 D. Malchow, R. Schaloske and C. Schlatterer, *Biochem. J.*, 1996, **319**(1), 323–327.
27 D. Malchow, R. Mutzel and C. Schlatterer, *Int. J. Dev. Biol.*, 1996, **40**, 135–139.
28 C. Schlatterer and R. Schaloske, *Biochem. J.*, 1996, **313**(2), 661–667.
29 K. Gottmann and C. J. Weijer, *J. Cell Biol.*, 1986, **102**, 1623–1629.
30 P. M. Janssens and P. J. Van Haastert, *Microbiol. Rev. Biol. Rev.*., 1987, **51**, 396–418.
31 L. Aubry and R. Firtel, *Annu. Rev. Cell Dev. Biol.*, 1999, **15**, 469–517.
32 G. N. Europe-Finner and P. C. Newell, *J. Cell Sci.*, 1987, **87**(2), 221–229.
33 G. N. Europe-Finner and P. C. Newell, *J. Cell Sci.*, 1986, **82**, 41–51.
34 G. N. Europe-Finner, S. J. McClue and P. C. Newell, *FEMS Microbiol. Lett.*, 1984, **21**, 21–25.
35 J. L. Milne and P. N. Devreotes, *Mol. Biol. Cell*, 1993, **4**, 283–292.
36 E. Alvarez-Curto, K. E. Weening and P. Schaap, *Biochem. J.*, 2007, **401**, 309–316.
37 K. Boeckeler, K. Adley, X. Xu, A. Jenkins, T. Jin and R. S. Williams, *Eur. J. Cell Biol.*, 2006, **85**, 1047–1057.
38 I. Bezprozvanny, J. Watras and B. E. Ehrlich, *Nature*, 1991, **351**, 751–754.
39 L. Song, S. M. Nadkarni, H. U. Bodeker, C. Beta, A. Bae, C. Franck, W. J. Rappel, W. F. Loomis and E. Bodenschatz, *Eur. J. Cell Biol.*, 2006, **85**, 981–989.
40 N. V. Valeyev, A. K. Downing, A. I. Skorinkin, I. D. Campbell and N. V. Kotov, *In Silico Biol.*, 2006, **6**, 545–572.
41 J. Lee, A. Ishihara, G. Oxford, B. Johnson and K. Jacobson, *Nature*, 1999, **400**, 382–386.
42 A. A. Bominaar, F. Kesbeke and P. J. Van Haastert, *Biochem. J.*, 1994, **297**(1), 181–187.
43 A. A. Bominaar and P. J. Van Haastert, *Biochem. J.*, 1994, **297**(1), 189–193.
44 A. Korthol, J. S. King, I. Keizer-Gunnink, A. J. Harwood and P. J. Van Haastert, *Mol. Biol. Cell*, 2007, **18**, 4772–4779.

View Online

45 P. W. Kriebel and C. A. Parent, *IUBMB Life*, 2004, **56**, 541–546.
46 T. Nebl and P. R. Fisher, *J. Cell Sci.*, 1997, **110**(22), 2845–2853.
47 N. V. Valeyev, P. Heslop-Harrison, I. Postlethwaite, N. V. Kotov and D. G. Bates, *Mol. BioSyst.*, 2008, **4**, 66–73.
48 N. V. Valeyev, P. Heslop-Harrison, I. Postlethwaite, A. N. Gizatullina, N. V. Kotov and D. G. Bates, *Mol. BioSyst.*, 2009, **5**, 43–51.
49 G. Gerisch and B. Hess, *Proc. Natl. Acad. Sci. U. S. A.*, 1974, **71**, 2118–2122.
50 J. Bumann, B. Wurster and D. Malchow, *J. Cell Biol.*, 1984, **98**, 173–178.
51 P. R. Fisher and Z. Wilczynska, *FEMS Microbiol. Lett.*, 2006, **257**, 268–277.
52 H. Flaadt, E. Jaworski and D. Malchow, *J. Cell Sci.*, 1993, **105**(4), 1131–1135.
53 D. Malchow, D. F. Lusche, A. De Lozanne and C. Schlatterer, *Cell Calcium*, 2008, **43**, 521–530.
54 Z. Wilczynska, K. Happle, A. Muller-Taubenberger, C. Schlatterer, D. Malchow and P. R. Fisher, *Eukaryot. Cell*, 2005, **4**, 1513–1525.
55 F. Wuytack and L. Raeymaekers, *J. Bioenerg. Biomembr.*, 1992, **24**, 285–300.
56 D. E. Evans, *Cell Calcium*, 1994, **15**, 241–246.
57 J. Rietdorf, F. Siegert and C. J. Weijer, *Dev. Biol.*, 1998, **204**, 525–536.
58 S. Bader, A. Kortholt, H. Snippe and P. J. Van Haastert, *J. Biol. Chem.*, 2006, **281**, 20018–20026.
59 A. Bhatt, I. Kaverina, C. Otey and A. Huttenlocher, *J. Cell Sci.*, 2002, **115**, 3415–3425.
60 R. A. Brundage, K. E. Fogarty, R. A. Tuft and F. S. Fay, *Science*, 1991, **254**, 703–706.
61 R. A. Brundage, K. E. Fogarty, R. A. Tuft and F. S. Fay, *Am. J. Physiol.*, 1993, **265**, C1527–1543.
62 J. Kim, D. G. Bates, I. Postlethwaite, L. Ma and P. A. Iglesias, *IEE Proc. Syst. Biol.*, 2006, **153**, 96–104.
63 P. W. Marks and F. R. Maxfield, *J. Cell Biol.*, 1990, **110**, 43–52.
64 P. W. Marks, B. Hendey and F. R. Maxfield, *J. Cell Biol.*, 1991, **112**, 149–158.
65 G. Giannone, P. Ronde, M. Gaire, J. Haiech and K. Takeda, *J. Biol. Chem.*, 2002, **277**, 26364–26371.
66 G. Giannone, P. Ronde, M. Gaire, J. Beaudouin, J. Haiech, J. Ellenberg and K. Takeda, *J. Biol. Chem.*, 2004, **279**, 28715–28723.
67 K. L. O'Connor, L. M. Shaw and A. M. Mercurio, *J. Cell Biol.*, 1998, **143**, 1749–1760.
68 J. Kim, P. Heslop-Harrison, I. Postlethwaite and D. G. Bates, *PLoS Comput. Biol.*, 2007, **3**, e218.
69 M. Planck, *Ann. Phys. Chem.*, 1890, **275**, 161.
70 W. Nernst, *Z. Physik. Chem.*, 1889, **4**, 129.
71 B. Hille, *Ionic Channels of Excitable Membranes*, Sinauer Associates, Sunderland, 1992.
72 I. Bosanac, T. Michikawa, K. Mikoshiba and M. Ikura, *Biochim. Biophys. Acta: Mol. Cell Res.*, 2004, **1742**, 89–102.
73 M. Pupillo, R. Insall, G. S. Pitt and P. N. Devreotes, *Mol. Biol. Cell*, 1992, **3**, 1229–1234.
74 P. N. Devreotes, *Neuron*, 1994, **12**, 235–241.
75 P. Schaap, R. Brandt and S. van Es, *Dev. Biol.*, 1995, **168**, 179–188.
76 F. I. Comer, C. K. Lippincott, J. J. Masbad and C. A. Parent, *Curr. Biol.*, 2005, **15**, 134–139.
77 M. A. Brandon and G. J. Podgorski, *Mol. Biol. Cell*, 1997, **8**, 1677–1685.
78 N. V. Valeyev, D. G. Bates, P. Heslop-Harrison, I. Postlethwaite and N. V. Kotov, *BMC Syst. Biol.*, 2008, **2**, 48.

Downloaded by University of Northumbria on 15 October 2012
Published on 16 April 2009 on http://pubs.rsc.org | doi:10.1039/B822074C

 This journal is © The Royal Society of Chemistry 2009